Generalized Space-Time-Periodic Diffraction Gratings: Theory and Applications

Sajjad Taravati* and George V. Eleftheriades
The Edward S. Rogers Sr. Department of Electrical and Computer Engineering, University of Toronto, Toronto, Ontario M5S 3H7, Canada

(Received 26 February 2019; revised manuscript received 4 July 2019; published 14 August 2019; corrected 28 October 2020)

This paper studies the theory and applications of the diffraction of electromagnetic waves by space-time-periodic (STP) diffraction gratings. We show that, in contrast with conventional spatially periodic gratings, a STP diffraction grating produces spatial diffraction orders, each of which is formed by an infinite set of temporal diffraction orders. Such spatiotemporally periodic gratings are endowed with enhanced functionalities and exotic characteristics, such as an asymmetric diffraction pattern, nonreciprocal and asymmetric transmission and reflection, and an enhanced diffraction efficiency. The theory of the wave diffraction by STP gratings is formulated through satisfying the conservation of both momentum and energy, as well as rigorous Floquet mode analysis. Furthermore, the theoretical analysis of the structure is supported by time- and frequency-domain finite-difference time-domain (FDTD) numerical simulations for both transmissive and reflective STP diffraction gratings. Additionally, we provide the conditions for Bragg and Raman-Nath diffraction regimes for STP gratings. Finally, as a particular example of a practical application of the STP diffraction gratings to communication systems, we propose an original multiple-access communication system featuring full-duplex operation. STP diffraction gratings are expected to find exotic practical applications in communication systems, especially for the realization of enhanced-efficiency or full-duplex beam coders, nonreciprocal beam splitters, nonreciprocal and enhanced-resolution holograms, and illusion cloaks.

DOI: 10.1103/PhysRevApplied.12.024026

I. INTRODUCTION

Light diffraction by spatially periodic structures is a fundamental phenomenon in optics and is of great importance in a variety of engineering applications [1]. Such spatially periodic diffraction gratings are formed by a slab with a periodic spatial variation at the wavelength scale. The form of the grating periodicity is usually sinusoidal [2,3] or binary [4]. They exhibit unique spectral properties as the light impinging on the periodically modulated medium is reflected or transmitted at specific angles only, which in general is not the case for aperiodic media. Diffraction gratings play the main role in numerous electromagnetic systems [5,6], including, but not restricted to holography [7,8], beam shaping [9], data processing and optical logic [10,11], medical diagnostic measurements [12,13], and microwave and optical spectrum analysis [14–16].

Over the past decade, STP media have spurred a huge amount of scientific attention, due to their extraordinary interaction with electromagnetic waves [17–26]. Such media are not governed by the Lorentz reciprocity law, so that they may provide a nonreciprocal frequency generation and amplification. Analytical investigation of wave propagation and scattering in time-periodic media [27–30] and STP media [19,20,23,31–35] represents an interesting topic due to the complexity and rich physics of the problem. Moreover, an interesting feature is the diverse and unique practical applications of STP media. As of today, STP structures have been used as parametric traveling-wave amplifiers [31,32,34,36,37], optical isolators and circulators [19,26,38–42], nonreciprocal metasurfaces [43–47], pure frequency mixers [48], antennas [49–54], impedance matching structures [55], and mixer-duplexer-antenna systems [56].

The key contributions of this paper are as follows:

(a) Despite the recent surge of scientific interest on exploring outstanding and unique properties and applications of STP media [19–24,26,28,30,34,41–46,48,50–59], there is still a lack of information on the operation of STP media in the diffraction regime. Here, we first introduce the concept of generalized periodic gratings. Such gratings are varying in both space and time, representing the generalized version of standard conventional static (time-invariant) spatially varying gratings. Next, we provide a deep analysis on the functionality of STP gratings in the diffraction regime based on the modal analysis for electromagnetic waves inside a STP grating and the wave-vector-diagram analysis for diffracted waves outside the STP grating.

*sajjad.taravati@utoronto.ca

 © 2019 American Physical Society

(b) We derive the electromagnetic wave diffraction from STP gratings and show that such gratings provide an infinite number of spatial diffraction orders, each of which is composed of an infinite number of temporal diffraction orders. Such a unique spatial-temporal diffraction mechanism occurs even upon incidence of a monochromatic wave on the STP grating.

(c) It is shown that each single spatial-temporal diffraction order is diffracted at a distinct angle of diffraction, corresponding to a distinct wave amplitude. The provided general analysis is applicable to all types of periodicities, e.g., binary and sawtooth periodic gratings. In addition, the presented generalized analytical solution can be applied to spatial time-invariant gratings, spatially invariant temporal gratings, and spatial-temporal gratings.

(d) It is demonstrated that, in contrast to conventional spatially periodic static gratings [6,16,60–64], in a STP grating each spatial diffraction order is composed of an infinite number of temporal harmonics, each one of which is diffracted at a certain angle of diffraction.

(e) We show that a STP grating provides various functionalities, such as nonreciprocal and angle-(or system-) asymmetric wave diffraction, an asymmetric diffraction pattern and frequency conversion, which may be used to realize new optical and communication systems with enhanced efficiency.

(f) The impact of the thickness of the STP grating on the diffraction mechanism is studied. It is shown that by varying the thickness of a STP grating, two completely different operation regimes, that is, Bragg (thick) and Raman-Nath (thin) regimes, can be achieved. The analytical formulas for the characteristics of these two regimes, as well as the efficiency and operation of these gratings, are provided.

(g) We investigate the wave diffraction in both transmissive and reflective STP diffraction gratings. In particular, we present the asymmetric and nonreciprocal diffraction transmission in a transmitted STP grating and angle-asymmetric and nonreciprocal diffraction reflection in a reflective STP grating. We show that, in contrast to the transmissive STP grating, a reflective STP grating provides strong diffraction orders even if its thickness is subwavelength. This is because a reflective STP grating offers a much stronger interaction with the incident wave in comparison with transmissive STP gratings.

(h) The provided theoretical analysis of general STP gratings is supported by finite-difference time-domain (FDTD) numerical simulations. We present both time- and frequency-domain results, which provide a strong tool for investigation and understanding of the wave diffraction from general STP gratings.

(i) We leverage some of the exotic properties and unique functionalities of STP diffraction gratings and present an advanced practical application. The proposed system is called a space-time diffraction code multiple-access (STDCMA) system, which is an original multiple-access communication system featuring full-duplex operation.

The paper is structured as follows. Section II presents the theoretical analysis of the wave diffraction from general STP diffraction gratings and derives the diffraction angles for each space-time diffracted order. In Sec. III, we provide illustrative examples supported by the FDTD numerical simulation investigation in the time and frequency domains as follows: Sec. III A investigates the wave diffraction from conventional static time-invariant gratings. Then, Sec. III B characterizes the STP grating and shows its asymmetric diffraction pattern for normal incidence. Section III B also evaluates the effect of the grating thickness on the wave diffraction. Subsequently, Sec. III C demonstrates the nonreciprocal and asymmetric diffraction introduced by transmissive and reflective STP gratings. Section IV presents practical applications of STP gratings by leveraging the unique and exotic properties of their diffraction pattern. Finally, Sec. V concludes the paper.

II. THEORETICAL ANALYSIS

A. Space-time-periodic diffraction grating

Figure 1(a) depicts the wave diffraction from conventional transmissive planar spatially periodic diffraction gratings. The conventional static grating in Fig. 1(a) possesses a relative electric permittivity in the region from $z = 0$ to $z = d$ given by $n_{\mathrm{gr}}^2(x) = \epsilon_{\mathrm{gr}}(x) = f_{\mathrm{per}}(x)$, where $f_{\mathrm{per}}(x)$ is a periodic function of x, e.g., a sinusoidal, binary (square), or sawtooth function. Electromagnetic waves always travel in straight lines, but when passing near an obstruction they tend to bend around that obstruction and spread out. The diffraction phenomenon occurs when an electromagnetic wave passes by a corner or through a slit or grating that has an optical size comparable to the wavelength. The diffraction by a grating is a specialized case of wave scattering, where an object with regularly repeating features yields an orderly diffraction of the electromagnetic wave in a pattern consisting of a set of diffraction orders m.

As shown in Fig. 1(a), considering normal incidence of the input wave ($\theta_i = 0$), a symmetric diffraction pattern with respect to $x = 0$ is produced by conventional static gratings, possessing a symmetric profile with respect to the $x = 0$ axis. An asymmetric diffraction pattern for normal incidence can be achieved by asymmetric static periodic metagratings [65,66]. However, gratings with symmetric and asymmetric profiles are both restricted by the Lorentz reciprocity theorem and, therefore, possess a reciprocal diffraction transmission response. The symemtry of the diffraction pattern in conventional periodic static gratings includes the symmetry in both the angles of diffraction orders θ_m (e.g., $\theta_{+2} = \theta_{-2}$) and the symmetry in the

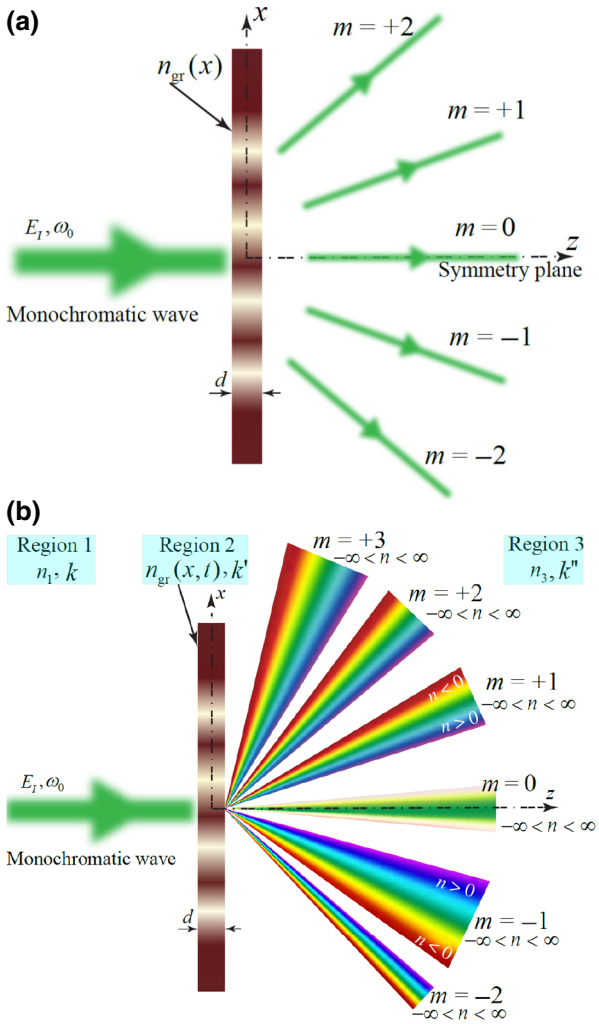

FIG. 1. Diffraction from a transmissive grating for a monochromatic incident wave. (a) Conventional spatial diffraction grating with $n_{gr}^2(x) = \epsilon_{gr}(x) = f_{per}(x)$, where spatial diffraction orders (e.g., $-2 < m < 2$) share the same temporal frequency, i.e., ω_0, with the input wave. (b) Generalized STP diffraction grating, i.e., $n_{gr}^2(x,t) = \epsilon_{gr}(x,t) = f\left[f_{1,per}(x), f_{2,per}(t)\right]$, where each mth spatial diffraction order (e.g., $-2 < m < 3$) is formed by an infinite number of temporal diffraction orders $\omega_0 + n\Omega$ with $-\infty < n < \infty$.

intensity of the diffracted orders P_m (e.g., $P_{+2} = P_{-2}$). In addition, assuming a monochromatic input wave with temporal frequency ω_0, no change in the temporal frequency of the incident field occurs and, hence, the diffracted orders share the same temporal frequency of ω_0.

Now, consider the transmissive planar STP diffraction grating shown in Fig. 1(b). This figure shows a generic representation of the spatiotemporal diffraction from a STP diffraction grating, which is distinctly different from the spatial diffraction from a conventional space periodic diffraction grating in Fig. 1(a). The grating is interfaced with two semi-infinite dielectric regions, i.e., region 1, characterized with the refractive index n_1 and wave number k, and region 3, characterized with the refractive index n_3 and wave number k''. The relative electric permittivity of this STP grating is periodic in both space and time, with temporal frequency Ω and spatial frequency K, given by

$$n_{gr}^2(x,t) = \epsilon_{gr}(x,t) = f\left[f_{1,per}(x), f_{2,per}(t)\right], \qquad (1)$$

where $f_{1,per}(x)$ and $f_{2,per}(t)$ are periodic functions of space (in the x direction) and time, respectively. The wave number in region 2 (inside the STP grating) is denoted by k'.

Assuming normal (or oblique) incidence of the input wave, the spatiotemporally periodic gratings [shown in Fig. 1(b)] produce an asymmetric diffraction pattern with respect to $x = 0$. This asymmetry in the diffraction pattern is due to the asymmetric spatiotemporal profile of the structure provided by the space-time modulation. The asymmetry of the diffraction pattern extends to both the diffraction angles of diffracted orders θ_m (e.g., $\theta_{m=+2} \neq \theta_{m-2}$) and the intensities of the diffracted orders P_m (e.g., $P_{m=+2} \neq P_{m=-2}$). Furthermore, the time variation of the grating (with frequency Ω) results in the generation of new frequencies. Hence, assuming a monochromatic input wave with temporal frequency ω_0, an infinite set of temporal frequencies is generated inside the grating and diffracted, so that each spatial diffracted order (m) is composed of an infinite number of temporal diffraction orders n. As a result, for such a generalized STP diffraction grating, the diffraction characteristics are defined for each spatial-temporal diffracted order (mn) so that the diffracted order (mn) is transmitted at a specified angle θ_{mn}, attributed to the electric field E_{mn}^T.

To best investigate the wave diffraction by a space-time-varying grating, we first study the interaction of the electromagnetic wave with space and time interfaces, separately. Figure 2(a) sketches the Minkowski space-time diagram of a spatial interface between two media of refractive indices n_1 and n_2, respectively, in the plane (z, ct). This figure shows scattering of forward and backward fields and conservation of energy and momentum for different scenarios. The temporal axis of the Minkowski space-time diagram is scaled with the speed of light c and, therefore, is labeled by ct for changing the dimension of the addressed physical quantity from time to length, in accordance with the dimension associated to the spatial axes labeled z. This problem represents the conventional case of electromagnetic wave incidence and scattering from a spatial (static) interface, where $n(z < 0) = n_1$ and $n(z > 0) = n_2$. At this spatial boundary, the normal magnetic field $\mathbf{B}$, the normal electric field displacement $\mathbf{D}$, and the temporal frequency are preserved, but the wave number k changes; i.e., energy is preserved but momentum changes. As a result, the wave number of the forward transmitted wave in region 2 corresponds to $k_t^+ = n_1 k_i^+ / n_2$, whereas the temporal frequency

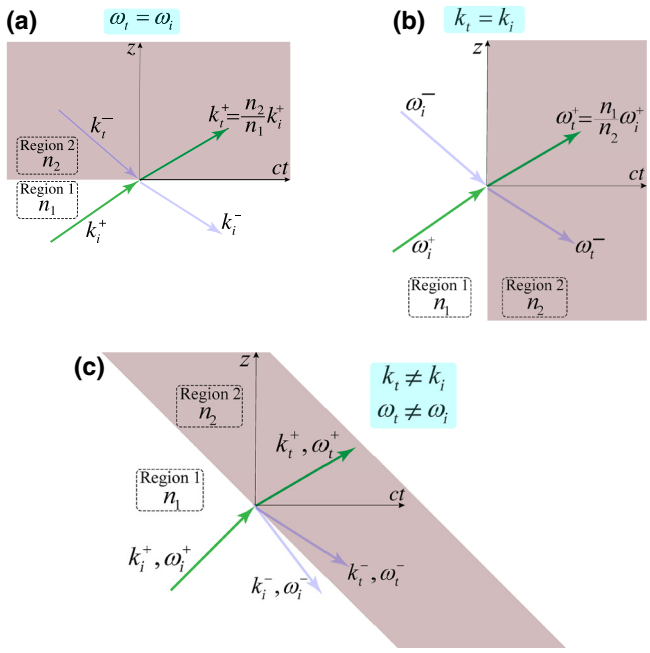

FIG. 2. Space-time diagrams showing scattering of forward and backward fields and conservation of energy and momentum for different scenarios. (a) Spatial interface, i.e., $n(z < 0) = n_1$ and $n(z > 0) = n_2$. (b) Temporal interface, i.e., $n(t < 0) = n_1$ and $n(t > 0) = n_2$. (c) Spatial-temporal interface, i.e., $n(z/c + t < 0) = n_1$ and $n(z/c + t > 0) = n_2$.

of the transmitted wave in region 2 is equal to that of region 1, i.e., $\omega_t = \omega_i$.

Figure 2(b) shows the space-time diagram of a time interface between two media of refractive indices n_1 and n_2, which is the dual case of the spatial slab in Fig. 2(a) [67–69]. Here, the refractive index suddenly changes from one value (n_1) to another (n_2) at a given time throughout all space, i.e., $n(t < 0) = n_1$ and $n(t > 0) = n_2$. The temporal change of the refractive index produces both reflected (backward) and transmitted (forward) waves, which is analogous to the reflected and transmitted waves produced at the spatial interface between two different media in Fig. 2(a). The total charge Q and the total flux ψ must remain constant at the moment of the jump from n_1 to n_2, implying that both transversal and normal components of **D** and **B** do not change instantaneously [70,71], which is different than the static case [shown in Fig. 2(a)] where only normal components of the magnetic field **B** and electric field displacement **D** are conserved. Specifically, at a time interface, the magnetic field **B**, the electric field displacement **D**, and the wave number k are preserved. This yields a change in the temporal frequency of the incident wave so that the frequency of the forward transmitted wave in region 2 corresponds to $\omega_t^+ = n_1\omega_i^+/n_2$, i.e., where momentum is preserved but energy changes.

Figure 2(c) depicts the space-time diagram of a spatial-temporal interface, i.e., $n(z/c + t < 0) = n_1$ and $n(z/c + t > 0) = n_2$, as the combination of the space and time interfaces in Figs. 2(a) and 2(a)(b), respectively. It may be seen that the spatial-temporal interface resembles the spatial interface configuration in Fig. 2(a) in the region $n = n_1$ and the temporal interface configuration in Fig. 2(b) for $n = n_2$. Here, only one of the four forward and backward waves reaches the interaction point from the past, whereas the other three waves travel from the interface in the positive time direction [68,72]. At such a spatial-temporal interface, the normal component of the magnetic field **B** and normal component of the electric field displacement **D** are preserved [73,74]. However, both the spatial frequency (wave number) k and the temporal frequency changes; i.e., both momentum and energy change. For a periodic space-time-modulated medium, as in Fig. 1(b), the same phenomenon, i.e., a change in the spatial and temporal frequencies, occurs for each interface. Hence, following the Floquet theorem, a STP grating introduces an infinite number of space and time diffraction orders, as described in Sec. II B.

B. Diffraction angles

Figure 3 shows a generic illustration example of a wave-vector isofrequency diagram for the diffraction from a STP diffraction grating. The grating is characterized with the spatial frequency K (the spatial periodicity of the STP grating reads $\Lambda = 2\pi/K$) and the temporal frequency Ω. Figure 3 sketches the phase matching of spatial-temporal harmonic components of the total field inside the grating with propagating backward-diffracted orders in region 1 and forward-diffracted orders in region 3. We assume the grating is interfaced with two semifinite dielectrics, i.e., $z \to -\infty <$ region $1 < z = 0$ and $d <$ region $3 < z \to \infty$, respectively. Region 1, region 2 (inside the STP grating), and region 3 are, respectively, characterized with the phase velocities $v_r = c/n_1$, $v_r' = c/n_{\rm av}$, and $v_r'' = c/n_3$ and the wave vectors $\mathbf{k}_{mn} = k_{x,mn}\hat{\mathbf{x}} + k_{z,mn}\hat{\mathbf{z}}$, $\mathbf{k}'_{pmn} = k'_{x,pmn}\hat{\mathbf{x}} + k'_{z,pmn}\hat{\mathbf{z}}$, and $\mathbf{k}''_{mn} = k''_{x,mn}\hat{\mathbf{x}} + k''_{z,mn}\hat{\mathbf{z}}$. Here, c represents the velocity of the light in the vacuum; m and n denote the number of the space and time harmonics, respectively; and p represents the number of the mode in region 2, inside the grating (these modes only exist inside the grating, and Sec. II D elaborates on their properties).

The STP grating assumes oblique incidence of a y-polarized electric field, with temporal frequency ω_0 and under an angle of incidence θ_i with respect to the normal of the grating, i.e.,

$$\mathbf{E}_i(x, z, t) = \hat{\mathbf{y}} E_0 e^{i(k_{x,i}x + k_{z,i}z - \omega_0 t)}, \tag{2}$$

where E_0 is the amplitude of the incident wave. In Eq. (2), $k_{x,i} = k_0 \sin(\theta_i) = \omega_0 \sin(\theta_i)/v_r$ and $k_{z,i} = k_0 \cos(\theta_i)$ are the x and z components of the incident wave vector, respectively.

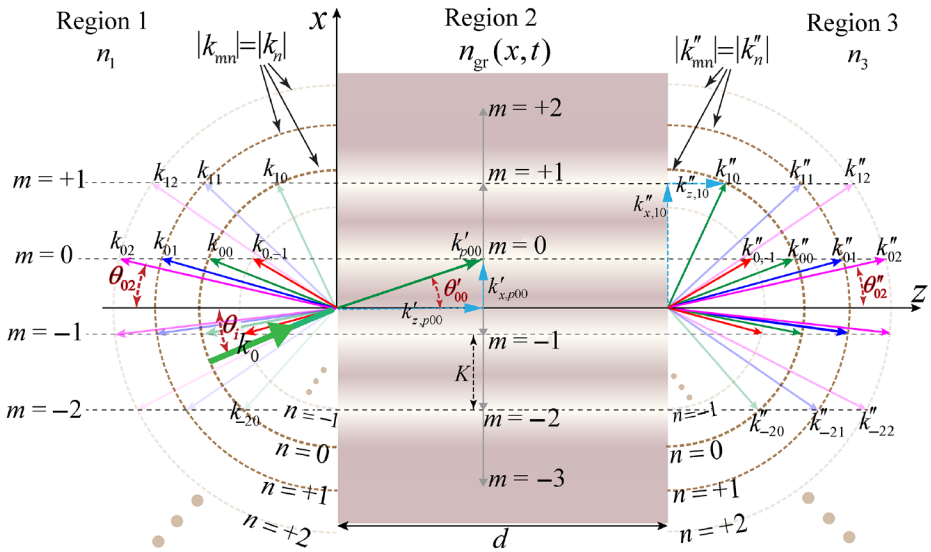

FIG. 3. Wave-vector isofrequency diagram for the diffraction from a STP diffraction grating, exhibiting phase matching of spatial-temporal harmonic components of total field inside the grating with propagating backward-diffracted orders in region 1 and forward-diffracted orders in region 3. The diffracted spatial-temporal harmonics corresponding to $-1 < m < +2$ is propagating diffracted orders, whereas the harmonics corresponding to $m < -1$ and $m > +2$ is evanescent (cut off) outside the STP grating.

The x component of the wave vector outside the STP grating, in region 3, reads

$$k''_{x,mn} = k''_n \sin(\theta''_{mn}), \tag{3}$$

where

$$k''_n = k''_0 + n\frac{\Omega}{v''_r}, \tag{4}$$

and where $k''_0 = \omega_0/v''_r$. The corresponding z component of the wave vector in region 3 is calculated using the Helmholtz relation, as

$$k''_{z,mn} = \sqrt{(k''_{mn})^2 - (k''_{x,mn})^2} = k''_n \cos(\theta''_{mn}). \tag{5}$$

The x and z components of the wave vector in region 1 ($k_{x,mn}$ and $k_{z,mn}$) and inside the grating ($k'_{x,mn}$ and $k'_{z,mn}$) can be achieved following the same procedure as in Eqs. (4) and (5). The space-time diffraction process may be simply interpreted as follows. The incident wave is refracted into the grating medium at $z = 0$, while generating an infinite set of time harmonics inside the grating, with frequencies $\omega_n = \omega_0 + n\Omega$ corresponding to the wave vectors $k'_n = k'_0 + n\Omega/v'_r$. The refracted space-time plane waves in the grating are diffracted into an infinite set of plane waves traveling toward the $z = d$ boundary. The space-time harmonic waves inside the grating are phase matched into propagating and evanescent waves in region 3; i.e., the x components of the wave vectors of the mth mode in regions 1 and 3 and the x component of the wavevector of the mth space-time harmonic field in region 2 must be the same.

To determine the spatial and temporal frequencies of the diffracted orders, we consider the momentum conservation law, i.e.,

$$k_{x,\mathrm{diff}} = k_{x,\mathrm{inc}} + mK \tag{6a}$$

or

$$k''_{x,mn} = k_{x,mn} = k_{x,i} + mK, \tag{6b}$$

and the energy conservation law, i.e.,

$$\omega_{\mathrm{diff}} = \omega_{\mathrm{inc}} + n\Omega \tag{6c}$$

or

$$\omega_n = \omega_0 + n\Omega, \tag{6d}$$

where $k_{x,\mathrm{diff}}$ and $k_{x,\mathrm{inc}}$ denote the x components of the wave vector of the diffracted and incident fields, respectively, and ω_{diff} and ω_{inc} represent the temporal frequencies of the diffracted and incident fields, respectively. Equation (6b), using Eq. (4), may be written as

$$\left(k''_0 + n\frac{\Omega}{v''_r}\right)\sin\left(\theta''_{mn}\right) = k_0 \sin(\theta_i) + mK, \tag{7}$$

where $k_0 = n_1\omega_0/c$. Seeking for the angle of diffraction for the forward spatial-temporal diffracted orders in region 3, i.e., the mth spatial and nth temporal harmonic, yields

$$\sin\left(\theta''_{mn}\right) = \frac{n_1}{n_3}\frac{\sin(\theta_i) + mK/k_0}{1 + n\Omega/\omega_0}. \tag{8}$$

The corresponding angle of diffraction for the backward-diffracted orders in region 1 reads

$$\sin\left(\theta_{mn}\right) = \frac{\sin(\theta_i) + mK/k_0}{1 + n\Omega/\omega_0}. \tag{9}$$

C. Propagating and evanescent orders

For a given set of incident angles, spatial and temporal frequencies of the grating, and the wavelength of the incident beam, the grating equation in Eq. (6b) may be satisfied for more than one value of m and n. However, there exists a solution only when $|\sin(\theta_{mn})| < 1$. Diffraction orders corresponding to m and n satisfying this condition are called "propagating" orders. The other orders yielding $|\sin(\theta_{mn})| > 1$ correspond to imaginary z components of the wave vector $k_{z,mn}$ as well as complex angles of diffraction $\sin(\theta_{mn})$. These evanescent orders decrease exponentially with the distance from the grating and, hence, can be detected only at a distance less than a few wavelengths from the grating. However, these evanescent orders play a key role in some surface-enhanced grating properties and are taken into account in the theory of gratings. Evanescent orders are essential in some special applications, such as, for instance, waveguide and fiber gratings. The specular order ($m = 0$) is always propagating, while the others can be either propagating or evanescent. The modulations with $2\pi/K \ll \lambda_0$ produce evanescent orders for $m \neq 0$, while the modulations with $2\pi/K \gg \lambda_0$ yield a large number of propagating orders.

In the homogeneous regions, i.e., regions 1 and 3, the magnitudes of the wave vectors of the backward- and forward-diffracted orders read

$$|k_{mn}| = |k_n| \quad \text{and} \quad |k''_{mn}| = |k''_n|. \tag{10}$$

As explained before, the x components of the diffracted wave vectors, $k_{x,mn}$ and $k''_{x,mn}$, can be deduced from the phase-matching requirements. Then, the propagating and evanescent nature of the corresponding orders is specified based on $k_{z,mn}$ and $k''_{x,mn}$, as follows. The real $k_{z,mn}$'s and $k''_{z,mn}$'s correspond to propagating orders, whereas the imaginary $k_{z,mn}$'s and $k''_{z,mn}$'s correspond to evanescent orders. The propagating and evanescent mth fields in regions 1 and 3 are shown in Fig. 3. The wave vectors in regions 1 and 3 possess magnitudes $|k_n|$ and $|k''_n|$, respectively. Hence, all spatial diffraction orders for the nth temporal harmonic in these two regions share the same amplitude, i.e., $|k_{mn}| = |k_n|$ and $|k''_{mn}| = |k''_n|$. Semicircles with these radii are sketched in Fig. 3. The allowed wave vectors in these regions must be phased matched to the boundary components of the spatial-temporal diffracted order inside the grating. This is shown by the horizontal dashed lines in the figure. In the qualitative illustration in Fig. 3, for the incident wave of wave vector k_0 and the grating with grating wave vector K and temporal frequency Ω, the $m = -1$ to $+2$ waves exist as propagating diffracted orders in regions 1 and 3. However, $m \leqslant -2$ and $m \geqslant +1$ are diffracted as evanescent orders.

D. Diffracted electromagnetic fields

The electromagnetic wave propagation and diffraction in general periodic media may be studied by several approaches. Among the proposed approaches, the modal approach [2,16,19,75] and the coupled-wave approach [4, 33] represent the most common and insightful approaches for analysis of periodic media diffraction gratings, both of which provide exact formulations without approximations. Here, we study the wave diffraction inside the STP grating using the modal approach. The modal approach has also been referred to as the Bloch-Floquet (or Floquet-Bloch), characteristic-mode, and eigenmode approach. Such an approach expresses the electromagnetic fields inside the grating as a combination of an infinite number of modes, each of those individually satisfying Maxwell's equations.

First, we expand the field inside the modulated medium in terms of the spatial-temporal diffracted orders (m and n) of the field in the periodic structure. This is due to the fact that the electromagnetic waves in periodic media take on the same periodicity as their host. These spatial-temporal diffracted orders inside the grating are phase matched to diffracted orders (either propagating or evanescent) outside of the grating. The partial space-time harmonic fields may be considered as inhomogeneous plane waves with a varying amplitude along the planar phase front. These inhomogeneous plane waves are dependent and they exchange energy back and forth between each other in the modulated grating.

Since the electric permittivity of the grating is periodic in both space and time, with spatial frequency K and temporal frequency Ω, it may be expressed in terms of the double Fourier series expansion as

$$n_{\mathrm{gr}}^2(x,t) = \epsilon_{\mathrm{gr}}(x,t) = \sum_m \sum_n \epsilon_{mn} e^{i(mKx - n\Omega t)}, \tag{11}$$

where ϵ_{mn} are complex coefficients of the permittivity and K and Ω are the spatial and modulation frequencies, respectively. The electric field inside the grating is expressed in terms of a sum of an infinite number of modes, i.e.,

$$\mathbf{E}_2(x,z,t) = \sum_{p=-\infty}^{\infty} \mathbf{E}_{2,p}(x,z,t). \tag{12}$$

Given the spatial-temporal periodicity of the grating, the corresponding electric field of the pth mode inside the grating may be decomposed into spatiotemporal Bloch-Floquet plane waves as

$$\mathbf{E}_{2,p}(x,z,t) = \hat{\mathbf{y}} \sum_m \sum_n E'_{pmn} e^{i(k'_{x,pmn}x + k'_{z,pmn}z - \omega_n t)}, \tag{13}$$

where

$$k'_{x,pmn} = k'_{x,p0n} + mK = \left(k'_{p00} + n\frac{\Omega}{v'_r}\right)\sin\left(\theta'_{p0n}\right) + mK \tag{14}$$

and

$$k'_{z,pmn} = k'_{pmn}\cos(\theta_i). \tag{15}$$

In Eq. (14), θ'_{p0n} reads

$$\theta'_{p0n} = \tan^{-1}\left(\frac{k'_{x,p0n}}{k'_{z,p0n}}\right). \tag{16}$$

The corresponding magnetic field inside the grating reads

$$\begin{aligned}\mathbf{H}_2(x,z,t) &= \frac{1}{\eta}\hat{\mathbf{k}}'_{pmn}\times\mathbf{E}_2(x,z,t)\\ &= \sum_{p,m,n}\left(-\hat{\mathbf{x}}\frac{k'_{z,pmn}}{k'_{pmn}} + \hat{\mathbf{z}}\frac{k'_{x,pmn}}{k'_{pmn}}\right)\\ &\quad\times\frac{E'_{pmn}}{\eta'}e^{i(k'_{x,pmn}x+k'_{z,pmn}z-\omega_n t)}.\end{aligned} \tag{17}$$

The unknown field coefficients E'_{pmn} and $k'_{x,p00}$ are to be found through satisfying Maxwell's equations, that is,

$$\nabla\times\mathbf{E}_2(x,z,t) = -\frac{\partial\mathbf{B}_2(x,z,t)}{\partial t}, \tag{18a}$$

$$\nabla\times\mathbf{H}_2(x,z,t) = \frac{\partial\mathbf{D}_2(x,z,t)}{\partial t}. \tag{18b}$$

The corresponding wave equation for the STP grating may be derived from Eqs. (18a) and (18b) and reads

$$\nabla^2\mathbf{E}_2(x,z,t) = \frac{1}{c^2}\frac{\partial^2}{\partial t^2}\left[\epsilon_{\mathrm{gr}}(x,t)\mathbf{E}_2(x,z,t)\right]. \tag{19}$$

We assume that the grating is invariant in the y direction (i.e., $\partial/\partial y = 0$). Then, inserting Eq. (12) into Eq. (19) yields

$$\begin{aligned}&\left(\frac{\partial^2}{\partial x^2}+\frac{\partial^2}{\partial z^2}\right)E'_{pmn}e^{i(k'_{x,pmn}x+k'_{z,pmn}z-\omega_n t)}\\ &= \frac{1}{c^2}\frac{\partial^2}{\partial t^2}\left(\sum_j\sum_q\epsilon_{jq}E'_{pmn}e^{i([k'_{x,pmn}+jK]x+k'_{z,pmn}z-[\omega_n+q\Omega]t)}\right)\\ &= \frac{1}{c^2}\frac{\partial^2}{\partial t^2}\sum_j\sum_q\epsilon_{m-j,n-q}E'_{pjq}e^{i(k'_{x,pmn}x+k'_{z,pmn}z-\omega_n t)}.\end{aligned} \tag{20}$$

Solving Eq. (20) for the unknown field coefficients E'_{pmn} gives

$$E'_{pmn} = \frac{(\omega_n/c)^2}{(k'_{x,pmn})^2+(k'_{z,pmn})^2}\sum_j\sum_q\epsilon_{m-j,n-q}E'_{pjq}. \tag{21}$$

Next, we determine the backward-diffracted fields in region 1 and forward-diffracted fields in region 3. As depicted in Fig. 3, one must consider the multiple backward- and forward-propagating diffracted orders that exist inside and outside of the grating. The total electric field in region 1 is the sum of the incident and the backward-traveling diffracted orders, given as

$$\mathbf{E}_1 = \hat{\mathbf{y}}E_0e^{i(k_{x,i}x+k_{z,i}z-\omega_0 t)} + \hat{\mathbf{y}}\sum_{m,n}E^R_{mn}e^{i(k_{x,mn}x-k_{z,mn}z-\omega_n t)}, \tag{22}$$

where E^R_{mn} is the unknown amplitude of the mth reflected spatial-temporal diffracted orders in region 1, with the wave vectors $k_{x,mn}$ and $k_{z,mn}$. The total electric field in region 3 reads

$$\mathbf{E}_3 = \hat{\mathbf{y}}\sum_{m,n}E^T_{mn}e^{i(k''_{x,mn}x+k''_{z,mn}z-\omega_n t)}, \tag{23}$$

where E^T_{mn} is the amplitude of the mth transmitted spatial-temporal diffracted order in region 3, with the wave vectors $k''_{x,mn}$ and $k''_{z,mn}$. To determine the unknown field coefficients of the backward- and forward-diffracted orders, E^R_{mn} and E^T_{mn}, we enforce the continuity of the tangential electric and magnetic fields at the boundaries of the grating at $z = 0$ and $z = d$. The electric field continuity condition between regions 1 and 2 at $z = 0$, $E_{1y}(x,0,t) = E_{2y}(x,0,t)$, using Eqs. (12) and (22), reduces to

$$\delta_{n0}E_0e^{ik_{x,i}x} + \sum_{m,n}E^R_{mn}e^{ik_{x,mn}x} = \sum_{p,m,n}E'_{pmn}e^{ik'_{x,pmn}x}, \tag{24}$$

and the corresponding magnetic field continuity condition, i.e., $H_{1x}(x,0,t) = H_{2x}(x,0,t)$, may be formulated as

$$\begin{aligned}&\cos(\theta_i)\delta_{m0}\delta_{n0}E_0e^{ik_{x,i}x} - \cos(\theta_{mn})E^R_{mn}e^{ik_{x,mn}x}\\ &= \eta_1\sum_p\frac{k'_{z,pmn}}{k'_{pmn}}\frac{E'_{pmn}}{\eta'}e^{ik'_{x,pmn}x}.\end{aligned} \tag{25}$$

The electric field continuity condition between regions 2 and 3 at $z = d$, $E_{2y}(x,d,t) = E_{3y}(x,d,t)$, reduces to

$$E^T_{mn} = \sum_p E'_{pmn}e^{i\left([k'_{x,pmn}-k''_{x,mn}]x+[k'_{z,pmn}-k''_{z,mn}]d\right)}, \tag{26}$$

while the corresponding tangential magnetic field continuity condition between regions 2 and 3 at $z = d$,

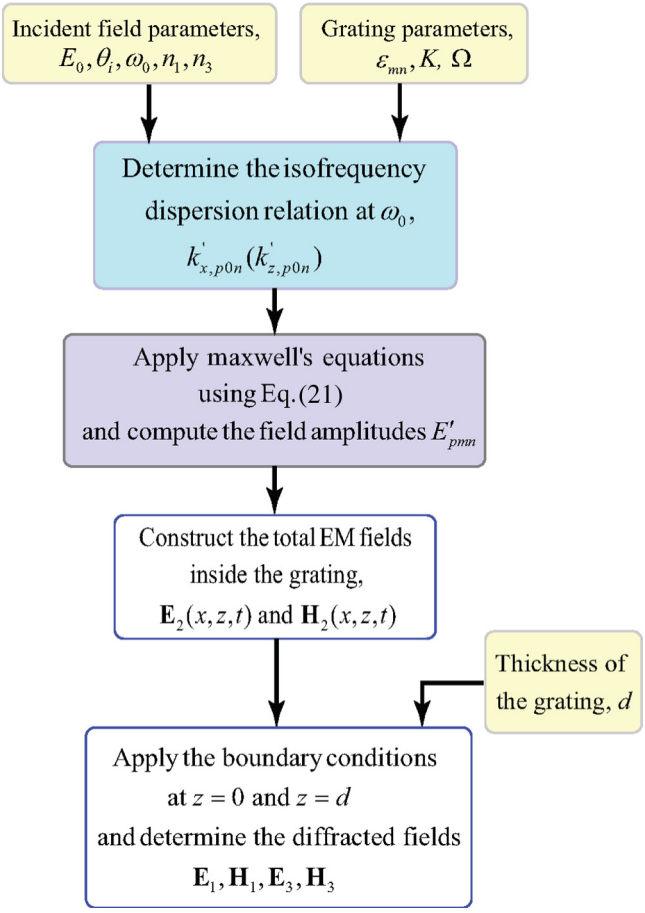

FIG. 4. Procedure for deriving the scattered electromagnetic fields inside and outside of a STP grating.

$H_{2x}(x,d,t) = H_{3x}(x,d,t)$, reads

$$\sum_p \frac{E'_{pmn}}{\eta'} e^{i\left([k'_{x,pmn}-k''_{x,mn}]x+[k'_{z,pmn}-k''_{z,mn}]d\right)} = \frac{\cos(\theta_{mn})}{\cos(\theta_i)} \frac{E^T_{mn}}{\eta''}. \tag{27}$$

Solving the above four equations, i.e., Eqs. (24)–(27), together provides the four unknown field amplitudes, i.e., the forward and backward field amplitudes inside the grating (E'^{+}_{pmn} and E'^{-}_{pmn}), and the reflected and transmitted field amplitudes outside the grating (E^R_{mn} and E^T_{mn}). Figure 4 overviews the procedure for determining unknown field amplitudes and the dispersion relation of a STP grating.

III. ILLUSTRATIVE EXAMPLES

A. Conventional spatially periodic static diffraction grating

For the sake of comparison, we first investigate the diffraction from a conventional planar spatially periodic (static) diffraction grating [1–3,16]. Such a static grating assumes a sinusoidal relative electric permittivity in the region from $z = 0$ to $z = d$, given by

$$n^2_{\rm gr}(x) = \epsilon_{\rm av} + \delta_\epsilon[1 + \sin(Kx)], \tag{28}$$

and interfaced with two semi-infinite dielectric regions, characterized with refractive indices n_1 and n_3, respectively. In Eq. (28), δ_ϵ represents the modulation strength. Figure 5 shows the time-domain FDTD simulation results for the diffraction from a conventional spatially periodic grating with $\theta_i = 0°$, $\omega_0 = 2\pi \times 10$ GHz, $\delta_\epsilon = 0.5$, $\Omega = 0$, $K = 0.4k_0$, $d = 0.8\lambda_0$. It may be seen from this figure that, for a monochromatic incident wave, all spatial diffracted orders possess the same wavelength (frequency). Another observed phenomenon is that, since the grating is "undirectional," the diffraction pattern for a normal incidence ($\theta_i = 0$) is symmetric with respect to the x axis. Table I lists the analytical results, derived from (8), for the diffraction angles θ_m (in degrees) of the conventional transmissive space periodic diffraction grating in Fig. 1(a).

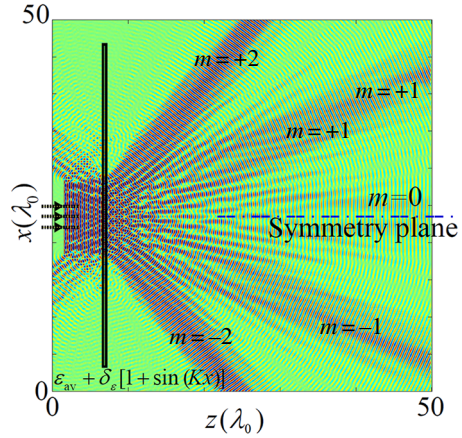

FIG. 5. FDTD numerical simulation results of the y component of the electric field for the diffraction from a conventional spatially periodic time-invariant grating ($\Omega = 0$), with $\theta_i = 0°$, $\omega_0 = 2\pi \times 10$ GHz, $\delta_\epsilon = 0.5$, $K = 0.4k_0$, $d = 0.8\lambda_0$.

B. Asymmetric pattern of a STP diffraction grating

Next, we demonstrate the diffraction from a planar STP (dynamic) diffraction grating. As a particular case, which

TABLE I. Analytical results for diffraction angles θ_m (in degrees) of the transmissive conventional spatially periodic time-invariant grating ($\Omega = 0$), corresponding to the FDTD numerical simulation results in Fig. 5. The evanescent spatiotemporal orders are represented by "Ev.".

m						
−3	−2	−1	0	+1	+2	+3
Ev.	−53.1	−23.58	0	23.58	53.1	Ev.

TABLE II. Analytical results for the diffraction angles θ_{mn} (in degrees) of the transmissive STP diffraction grating, where the FDTD numerical simulation results are given in Fig. 6. The dominant spatiotemporal diffraction orders, corresponding to $m = n$, are highlighted. The evanescent spatiotemporal orders are represented by "Ev.".

	m						
	-3	-2	-1	0	$+1$	$+2$	$+3$
$n = -3$	Ev.	Ev.	Ev.	0	Ev.	Ev.	Ev.
$n = -2$	Ev.	Ev.	-65.4	0	65.4	Ev.	Ev.
$n = -1$	Ev.	Ev.	**-33.7**	0	33.7	Ev.	Ev.
$n = 0$	-70	-38.7	-18.2	**0**	18.2	38.7	70
$n = +1$	-59	-34.85	-16.6	0	**16.6**	34.85	59
$n = +2$	-50.3	-30.8	-14.86	0	14.86	**30.8**	50.3
$n = +3$	-40.77	-25.8	-12.55	0	12.55	25.8	**40.7**

is practical and common, we study the grating with a sinusoidal relative electric permittivity in the region from $z = 0$ to $z = d$, given by

$$n_{\rm gr}^2(x,t) = \epsilon_{\rm av} + \delta_\epsilon[1 + \sin(Kx - \Omega t)]. \tag{29}$$

To compute the solution derived in Sec. II D, we shall write the expression in Eq. (29) in terms of its spatial-temporal Fourier components, considering the general form given in Eq. (11), i.e.,

$$n_{\rm gr}^2(x,t) = \epsilon_{-1,-1}e^{-j(Kx-\Omega t)} + \epsilon_{00} + \epsilon_{11}e^{+j(Kx-\Omega t)}, \tag{30a}$$

with

$$\epsilon_{11} = -\epsilon_{-1,-1} = \delta_\epsilon/2i \quad \text{and} \quad \epsilon_{00} = \epsilon_{\rm av} + \delta_\epsilon. \tag{30b}$$

We next insert the nonzero terms of the permittivity, given in Eq. (30b), into Eq. (21), and we determine the electromagnetic fields inside the grating, dispersion relation [19–21], and the diffracted fields. Table II lists the analytical results for the diffraction angles θ_{mn} (in degrees) of the transmissive STP diffraction grating, for normal incidence of a monochromatic wave, $\theta_i = 0°$, $\omega_i = \omega_0 = 2\pi \times 10$ GHz, where $\delta_\epsilon = 0.5$, $\Omega = 0.28\omega_0$, $K = 0.4k_0$, and $d = 0.8\lambda_0$.

Figure 6 shows the corresponding time-domain FDTD simulation results for the diffraction from this STP grating. We observe from this figure that, in contrast with the conventional case in Fig. 5, the diffraction pattern of the STP grating is asymmetric with respect to the x axis. The second observed phenomenon, as expected, is that the diffracted orders possess different wavelengths, which correspond to different frequencies. From Fig. 6, one may conclude that each diffracted order is attributed to a single frequency. However, this is not true. To see the exact phenomenon, we shall look at the frequency spectrum of the diffracted orders, by performing a fast Fourier transform of the transmitted diffracted orders at different angles.

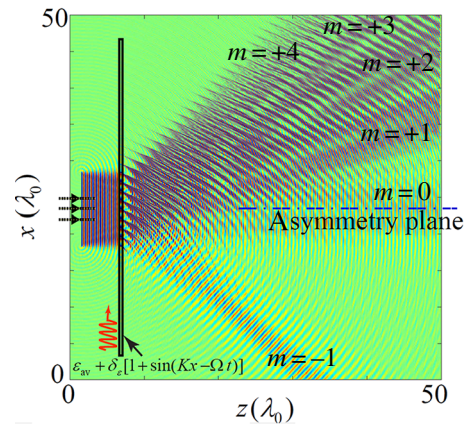

FIG. 6. Analytical and FDTD simulation results of the y component of the transmitted electric field, i.e., $E_{y,mn}^T$ for the spatial-temporal diffraction from a STP grating, for normal incidence of a plane wave ($\theta_i = 0°$) with temporal frequency $\omega_0 = 2\pi \times 10$ GHz, where $\delta_\epsilon = 0.5$, $\Omega = 0.28\omega_0$, $K = 0.4k_0$, $d = 0.8\lambda_0$. The analytical results for the angles of diffraction are listed in Table II.

Figures 7(a)–7(f) plot the analytical and FDTD numerical simulation frequency-domain responses for the $m = -1$ to $m = +4$ diffracted orders, corresponding to the analytical results listed in Table II. These figures show that each diffracted spatial order includes an infinite set of temporal harmonics, $\omega_n = \omega_0 + n\Omega$, with n being any integer. The animation of the time domain $E_{y,mn}(x,z,t)$ for the FDTD numerical simulation of the spatial-temporal diffraction from the STP grating in Fig. 6 is presented in Video 1.

1. Effect of the grating thickness

It is of great interest to investigate the effect of the thickness of the STP grating (d) on the generation of space and time diffraction orders and the grating efficiency. In

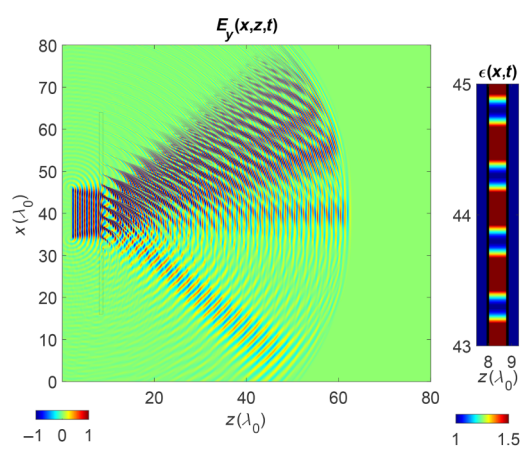

VIDEO 1. Animation of the time domain $E_{y,mn}(x,z,t)$ for the FDTD numerical simulation of the spatial-temporal diffraction from the STP grating in Fig. 6, for normal incidence of a plane wave.

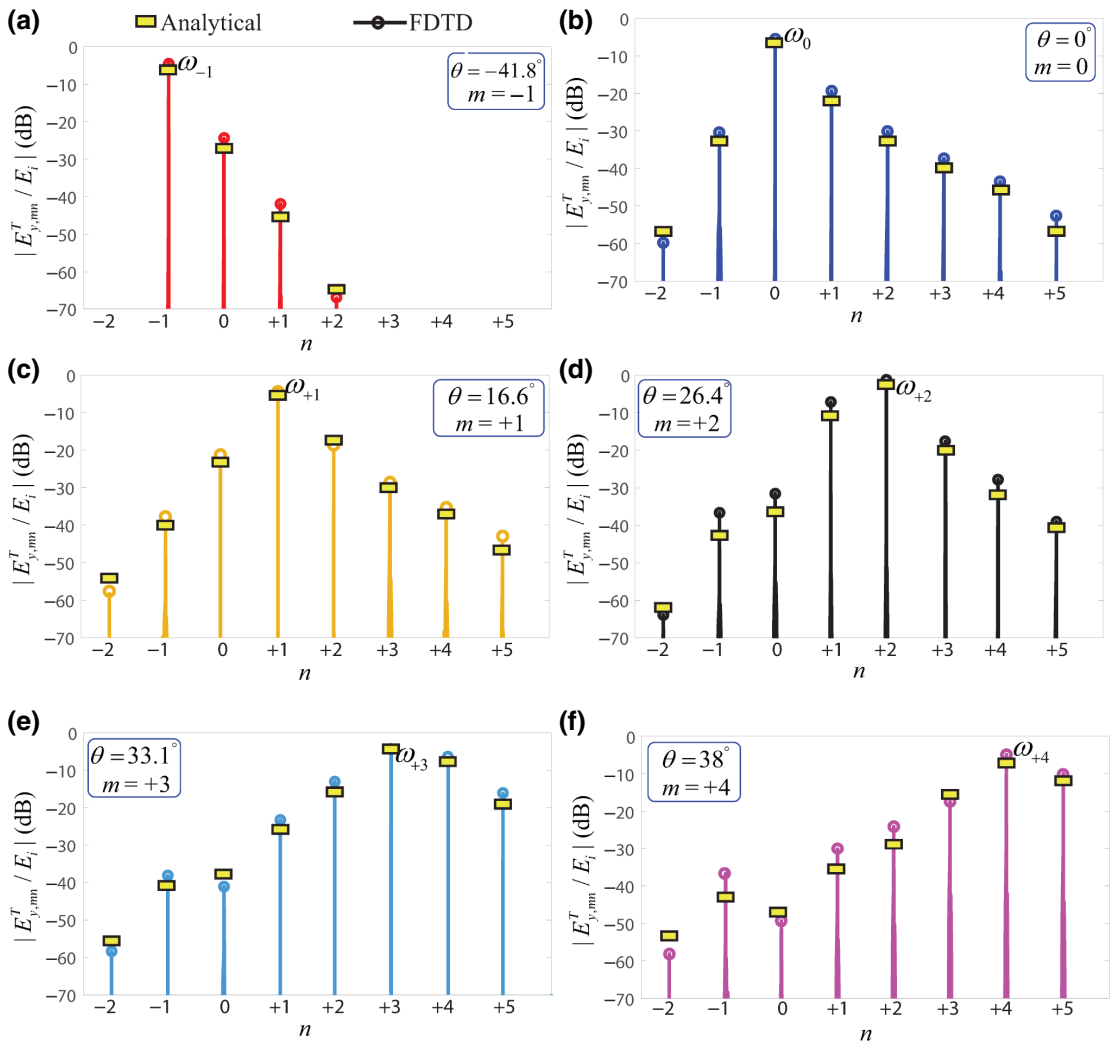

FIG. 7. Frequency-domain responses for spatial-temporal diffraction from the STP grating in Fig. 6: (a) $m = -1$, (b) $m = 0$, (c) $m = +1$, (d) $m = +2$, (e) $m = +3$, (f) $m = +4$.

general, diffraction gratings may be classified into two main categories, i.e., thin and thick gratings, each of which exhibits its own angular and wavelength selectivity characteristics. The thin gratings usually result in Raman-Nath regime diffraction, where multiple diffracted orders are produced. In contrast, the thick gratings usually result in Bragg regime diffraction, where only one single diffracted order is produced. Following the procedure described in Refs. [5] and [16], we characterize these two diffraction regimes, i.e., the Bragg and Raman-Nath regimes, by the dimensionless parameter

$$Q_n = \frac{v_r K^2 d}{(\omega_0 + n\Omega)\cos(\theta_n')}. \tag{31}$$

The grating strength parameter is represented by

$$\gamma_n = \frac{\delta_\epsilon}{\epsilon_{\text{av}}} \frac{d(\omega_0 + n\Omega)}{4 v_r \cos(\theta_n')} \tag{32}$$

for TE polarization and

$$\gamma_n = \frac{\delta_\epsilon}{\epsilon_{\text{av}}} \frac{d(\omega_0 + n\Omega)\cos(2\theta_n')}{4 v_r \cos(\theta_n')} \tag{33}$$

for TM polarization.

a. Thin STP grating (Raman-Nath regime). The required condition for thin STP gratings exhibiting Raman-Nath regime diffraction is represented by

$$Q_n \gamma_n \leq 1. \tag{34}$$

Thin gratings may also be characterized as gratings showing small angular and wavelength selectivity. As the incident wave is dephased (either in angle of incidence or in wavelength) from the Bragg condition, the diffraction efficiency decreases. The angular range or wavelength range for which the diffraction efficiency decreases to half of its on-Bragg-angle value is determined by the thickness of

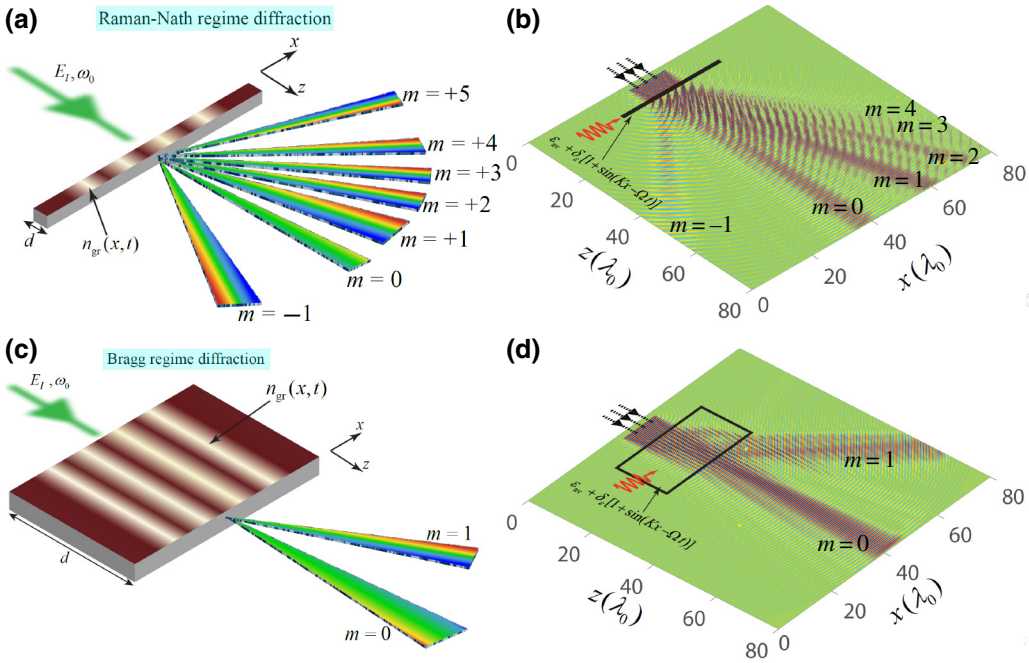

FIG. 8. Operation regimes of STP transmissive diffraction gratings, for normal incidence ($\theta_i = 0°$), $\omega_0 = 2\pi \times 10$ GHz. (a) Raman-Nath regime diffraction of a thin grating, where $\Omega = 0.4\omega_0$, $K = 0.4k_0$, $\delta_\epsilon = 0.5$, and $d = 0.5\lambda$. (b) Bragg regime diffraction of a thick grating, where $\Omega = 0.347\omega_0$, $K = 0.867k_0$, $\delta_\epsilon = 0.1$, and $d = 16\lambda$.

the grating d expressed as a number of grating periods $\Lambda = 2\pi/K$. For a thin grating, this number is reasonably chosen to be

$$Kd \leq 20\pi. \tag{35}$$

Figure 8(a) shows a generic representation of the Raman-Nath regime diffraction in STP transmissive diffraction gratings, for normal incidence ($\theta_i = 0°$), $\omega_0 = 2\pi \times 10$ GHz, $\Omega = 0.4\omega_0$, $K = 0.4k_0$, $\delta_\epsilon = 0.5$, and $d = 0.5\lambda$. Figure 8(b) shows the numerical simulation results for the Raman-Nath regime diffraction of the STP grating in Fig. 8(a). Following the procedure described in Refs. [5] and [16] (for conventional spatially periodic gratings), for a thin transmissive STP grating operating in the Raman-Nath regime, the diffraction efficiency reads

$$\eta_{mn} = \frac{P_{mn}}{P_{\text{inc}}} = J_m^2(2\gamma_n), \tag{36}$$

where P_{mn} and P_{inc} are the diffracted and incident powers, respectively, and where J represents the integer-order ordinary Bessel function of the first kind.

b. Thick STP grating (Bragg regime). The Bragg regime diffraction may be achieved in thick gratings, where the required condition is then

$$\frac{Q_n}{2\gamma_n} \geq 10. \tag{37}$$

Thick gratings are capable of exhibiting strong angular and wavelength selectivity. A relatively small change in the angle of incidence from the Bragg angle or a relatively small change in the wavelength at the Bragg angle may result in a relatively strong dephasing, which, in turn, decreases the diffraction efficiency. Thick grating behavior occurs when

$$Kd \geq 20\pi. \tag{38}$$

Figure 8(c) shows a generic representation of the Bragg regime diffraction in STP transmissive diffraction gratings, for normal incidence ($\theta_i = 0°$), $\omega_0 = 2\pi \times 10$ GHz, $\Omega = 0.4\omega_0$, $K = 0.4k_0$, $\delta_\epsilon = 0.5$, and $d = 0.5\lambda$. Figure 8(d) shows the numerical simulation results for Bragg regime diffraction of the STP grating in Fig. 8(c). Following the procedure described in Refs. [5] and [16] (for conventional spatially periodic gratings), for a thick transmissive STP grating operating in the Bragg regime, the diffraction efficiency reads

$$\eta_{1n} = \sin^2(2\gamma_n). \tag{39}$$

C. Asymmetric and nonreciprocal response of diffraction orders in STP gratings

Over the past few years, there has been a surge of interest in the nonreciprocal [19,20,33,43–45,76–78] and asymmetric [79–83] wave transmission, reflection, and absorption. Here, we investigate the realization of nonreciprocal, asymmetric, and angle-asymmetric wave diffraction by STP gratings. The spatial diffraction of electromagnetic waves by natural media is reciprocal under reversal of the incident wave direction, whereas asymmetric and nonreciprocal spatial diffraction of electromagnetic waves has been recently achieved using different

techniques [84–86]. It should be noted that asymmetry and nonreciprocity in electromagnetic systems are different. The main difference is that asymmetric structures, which are linear and time invariant, are constrained by the Lorentz reciprocity and cannot create optical isolators. For the sake of clarification, all time-invariant linear systems, represented by symmetric electric permittivity tensors and symmetric magnetic permeability tensors, are restricted by the Lorentz reciprocity theorem. Such systems are reciprocal as their scattering matrices are symmetric even if the electric permittivity tensor or the magnetic permeability tensor are complex (system introduces gain or loss).

The difference between the excitation and response for validation of the symmetry and reciprocity of electromagnetic systems, associated with new frequency generation, is clarified in Figs. 9(a) and 9(b). Figure 9(a) shows the forward and backward problems for the symmetry test of a particular symmetric electromagnetic system, where the backward problem is represented by the spatial inversion of the forward problem; i.e., the applied excitation wave (input) of the backward problem must be the spatial inversion of the excitation wave (input) of the forward problem. As a result, for a symmetric system, the output of the backward problem would be exactly the spatial inversion of the output of the forward problem. Otherwise, the system is asymmetric. Figure 9(b) shows the forward and backward problems for the reciprocity test of a particular reciprocal electromagnetic system, where the backward problem is the spatial inversion of the time-reversed forward problem; i.e., the applied excitation wave (input) of the backward problem must be the spatial inversion of the output of the forward problem. As a result, for a reciprocal system, the output of the backward problem would be exactly the spatial inversion of the input of the forward problem. Otherwise, the system is nonreciprocal.

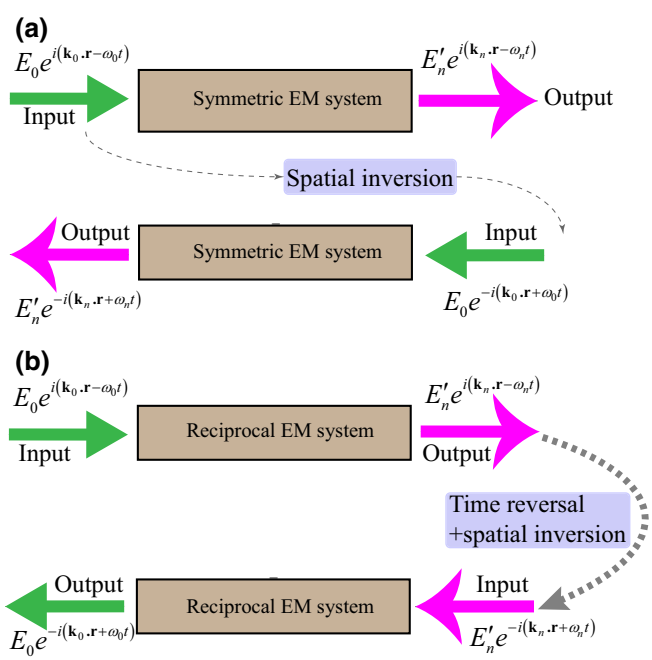

FIG. 9. Schematic of the experimental setup configurations for validation of symmetric and reciprocal response of electromagnetic systems. (a) The electromagnetic symmetry of the system is validated, in which the backward problem is the spatial inversion of the forward problem. (b) The electromagnetic reciprocity of the system is validated, in which the backward problem is the spatial inversion of the time-reversed forward problem.

Let us now elaborate on the nonreciprocal, asymmetric, and angle-asymmetric transmission and reflection of spatial-temporal diffractions introduced by STP gratings that can be used for the realization of a class of efficient telecommunication and optical systems.

1. Transmissive STP grating

Figure 10(a) illustrates a particular example, where a $+z$-propagating incident field (forward problem) obliquely impinges on a STP grating. The STP grating possesses an x-traveling space-time-varying permittivity $\epsilon(x,t) = \epsilon_{\text{av}} + \delta_\epsilon[1 + \sin(Kx - \Omega t)]$. Figure 10(b) shows the FDTD numerical simulation result of the transmissive diffraction by the STP diffraction grating in Fig. 10(a) with $\theta_i = 35^\circ$ and $\omega_0 = 2\pi \times 10$ GHz, where $\delta_\epsilon = 0.5$, $\Omega = 2\pi \times 4$ GHz, and $d = 0.8\lambda_0$. As expected, the diffracted spatial-temporal orders possess different wavelengths and different amplitudes. Next, we investigate the nonreciprocity of the STP grating in Fig. 10(b). Figures 10(c) and 10(d) show, respectively, the schematic and results of the backward problem for the reciprocity test of the grating. Following the procedure for the reciprocity test shown in Fig. 9(b), the backward problem is the spatial inversion of the time-reversed forward problem in Figs. 10(a). Therefore, the excitation input wave of the backward problem is the spatial inversion of the output of the forward problem, which is a polychromatic wave. As it is shown in Figs. 10(c) and 10(d), the output of the backward problem is completely different than (the spatial inversion of) the incident wave of the forward problem. Hence, the STP grating introduces nonreciprocal wave transmission.

Then, we investigate symmetrical diffraction transmission by the STP grating. Consider a $-z$-propagating incident field (backward wave incidence) that obliquely impinges on the same STP grating as in Figs. 10(a) and 10(b), but from the other side of the STP grating and under the angle of incidence $\theta_i = 35^\circ$. This scenario is depicted in Fig. 10(e) and the corresponding time-domain response is shown in Fig. 10(f). Comparing the numerical simulation results in Figs. 10(b) and 10(f), we see that the

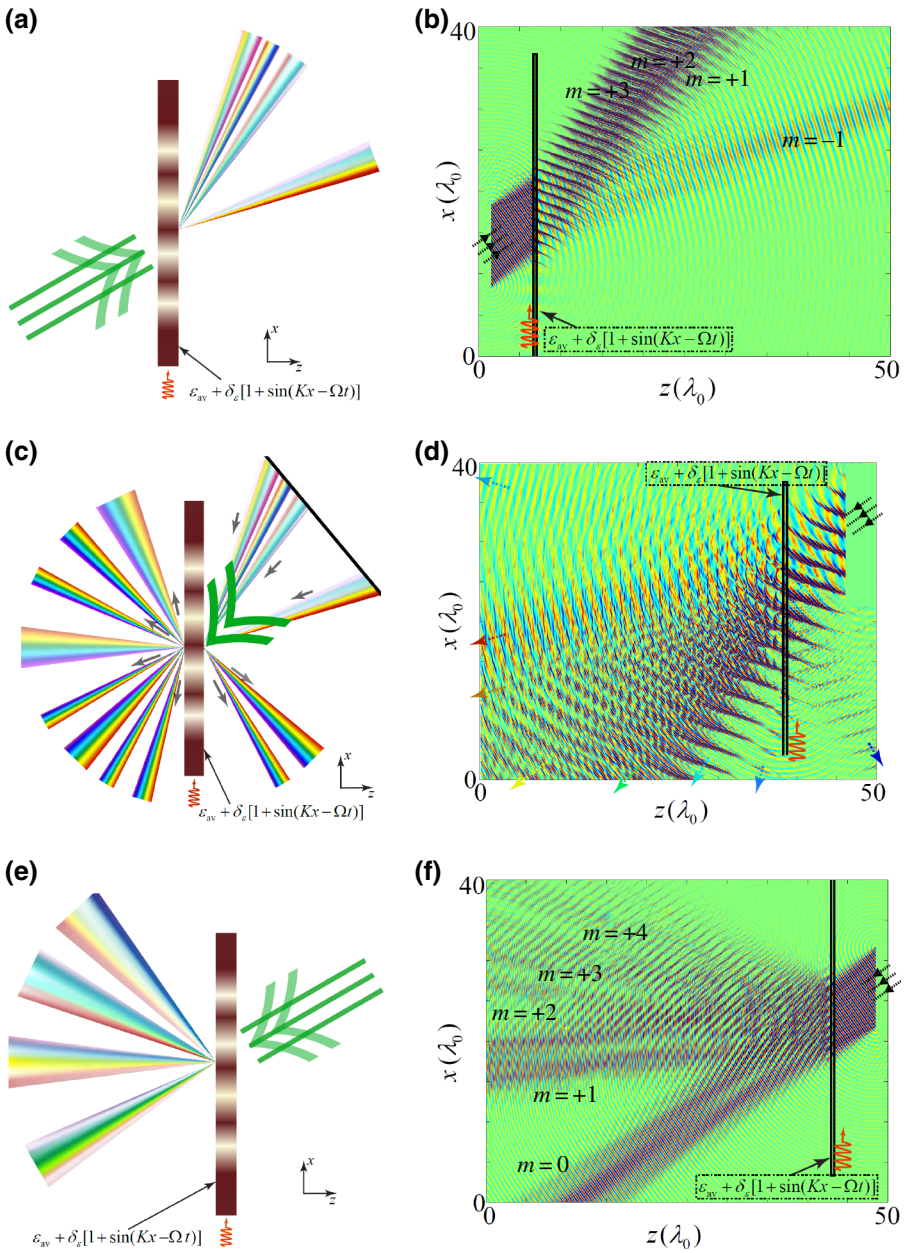

FIG. 10. Nonreciprocal and asymmetric wave diffraction from a transmissive STP grating with sinusoidal space-time-varying permittivity, i.e., $\epsilon(x,t) = \epsilon_{av} + \delta_\epsilon \sin(Kx - \Omega t)$, where $\theta_i = 35°$, $\omega_0 = 2\pi \times 10$ GHz, $\delta_\epsilon = 0.5$, $\Omega = 2\pi \times 4$ GHz, and $d = 0.8\lambda_0$. (a),(b) Forward problem. (c),(d) Backward problem for demonstration of nonreciprocal wave diffraction. (e),(f) Backward problem for demonstration of asymmetric wave diffraction.

STP grating introduces completely different diffraction patterns for forward and backward incidence. This includes the difference in the angle of diffraction and amplitude of the diffracted fields.

2. Reflective STP grating

Here, we study the operation of the STP diffraction grating in the reflective mode. Such a grating may be realized based on the combination of a STP diffraction grating and a metallic surface. Metals naturally reflect light with high efficiency, so that by integrating a STP grating and a metal, one may achieve a fully reflective STP diffraction grating. Figure 11(a) depicts a reflective STP grating, where a perfect electric conductor (PEC) is used at the bottom of the structure, providing full reflection of spatial-temporal diffractions. Figure 11(b) provides the numerical results for the diffraction by the grating in Fig. 11(a) for forward incidence, where $\theta_i = 35°$, and with an $+x$-traveling modulation, i.e., $\epsilon(x,t) = \epsilon_{av} + \delta_\epsilon[1 + \sin(Kx - \Omega t)]$, with $\omega_0 = 2\pi \times 10$ GHz, where $\delta_\epsilon = 0.5$, $\Omega = 2\pi \times 4$ GHz, and $d = 0.8\lambda_0$. Following the same operation as the transmissive STP grating, here the diffracted orders possess different wavelengths.

We next investigate the nonreciprocity of the reflective STP grating in Fig. 11(a). Figures 11(c) and 11(d) show, respectively, the schematic and numerical results of the backward problem for the reciprocity test of the

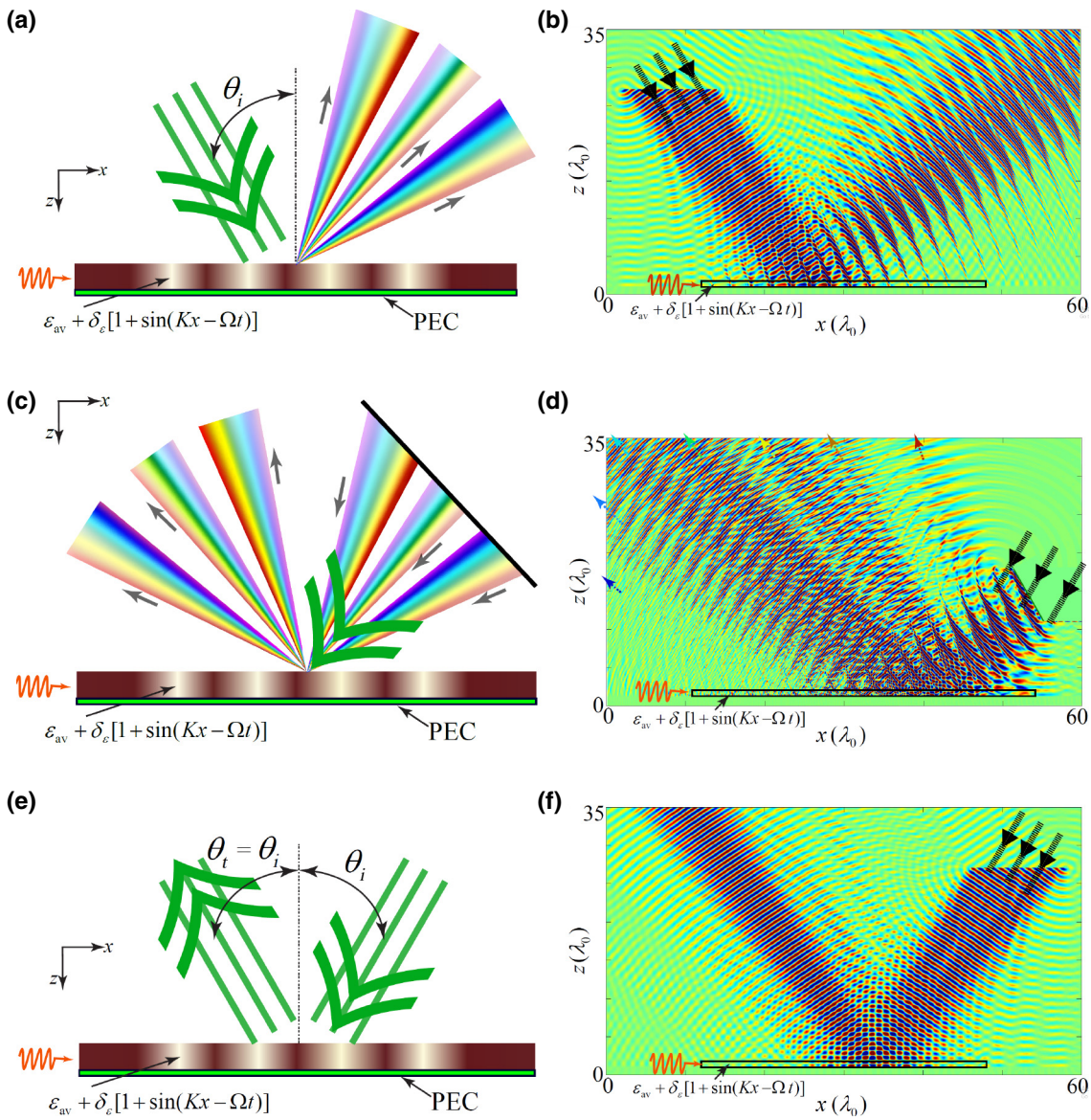

FIG. 11. Nonreciprocal and angle-asymmetric spatial-temporal diffraction of a reflective STP diffraction grating with a $+x$-traveling space-time-varying electric permittivity, i.e., $\epsilon(x,t) = \epsilon_{av} + \delta_\epsilon[1 + \sin(Kx - \Omega t)]$, where $\delta_\epsilon = 0.5$, $\Omega = 0.4\omega_0$, $d = 0.8\lambda_0$. (a),(b) Forward incidence, where $\theta_i = 35°$. (c),(d) Backward problem for demonstration of nonreciprocal wave diffraction. (e),(f) Backward problem for demonstration of angle-asymmetric wave diffraction, where $\theta_i = -35°$. The analytical results for the angle of diffraction are listed in Table III.

reflective grating. Following the procedure for the reciprocity test shown in Fig. 9(b), the backward problem is the spatial inversion of the time-reversed forward problem in Fig. 11(a). Thus, the excitation wave of the backward problem is the spatial inversion of the output of the forward problem, which is a polychromatic wave. It may be seen from Figs. 11(c) and 11(d) that the output of the backward problem is totally different than (the spatial inversion of) the incident wave of the forward problem, which demonstrates strong nonreciprocity of the reflective STP grating.

For the angle-symmetry test of the reflective grating in Fig. 11(a), we consider incidence of the wave under the angle of incidence $\theta_i = -35°$, as sketched in Fig. 11(e). The corresponding FDTD numerical simulation result is shown in Fig. 11(f). Comparing the results of the forward and backward incidence, shown in Figs. 11(b) and 11(f), respectively, one may obviously see that the reflective diffraction by the grating is completely angle asymmetric. Such an asymmetric reflective diffraction includes asymmetric angles of diffraction and unequal amplitudes of the diffracted orders. Figures 12(a)–12(d) plot the FDTD

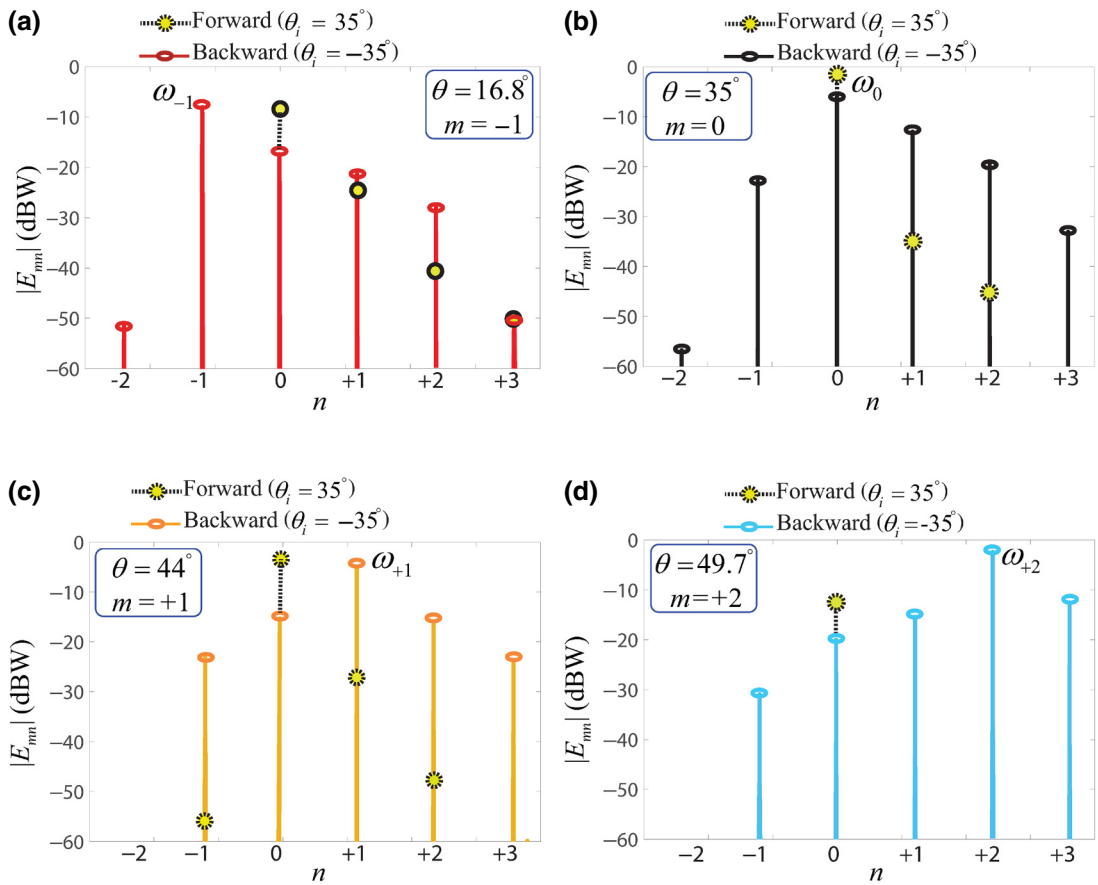

FIG. 12. Frequency spectrum of the diffracted orders for the forward problem in Figs. 11(a) and 11(b) ($\theta_i = 35°$) and the backward problem in Figs. 11(e) and 11(f) ($\theta_i = -35°$), exhibiting high isolation between diffraction orders of forward and backward problems.

numerical simulation frequency-domain responses for the $m = -1$ to $m = +2$ diffracted orders. Figure 13 plots the isolation of each spatial-temporal diffracted order for forward and backward incidences shown in Figs. 11(b) and 11(f), respectively. Table III lists the analytical results for the diffraction angles θ_{mn} (in degrees) of the reflective STP diffraction grating, considering an incident field impinging on the surface of the grating under the incident angle of

TABLE III. Analytical results for diffraction angles θ_{mn} (in degrees) of the reflective STP diffraction grating, where the FDTD numerical simulation results are given in Fig. 11. The evanescent spatiotemporal orders are represented by "Ev.".

		m						
	Incidence	−3	−2	−1	0	+1	+2	+3
$n = -3$	Forward	Ev.	Ev.	−60	Ev.	Ev.	Ev.	Ev.
	Backward	Ev.	Ev.	Ev.	Ev.	−60.2	Ev.	Ev.
$n = -2$	Forward	Ev.	Ev.	60	Ev.	Ev.	Ev.	Ev.
	Backward	Ev.	Ev.	Ev.	Ev.	60.2	Ev.	Ev.
$n = -1$	Forward	Ev.	−22.2	**16.8**	72.9	Ev.	Ev.	Ev.
	Backward	Ev.	Ev.	Ev.	73	16.8	−22.1	Ev.
$n = 0$	Forward	−38.8	−13.1	10	**35**	76.8	Ev.	Ev.
	Backward	Ev.	Ev.	76.8	**35**	10	−13	−38.8
$n = +1$	Forward	−26.6	−9.3	7.1	24.2	**44**	78.8	Ev.
	Backward	Ev.	78.8	44	24.2	**7.1**	−9.3	−26.6
$n = +2$	Forward	−20.4	−7.2	5.5	18.6	32.7	**49.7**	80.2
	Backward	80.2	49.7	32.7	18.6	5.5	**−7.2**	−20.4
$n = +3$	Forward	−16.5	−5.9	4.5	15.1	26.3	38.6	**53.7**
	Backward	53.7	38.6	26.3	15.1	4.5	−5.9	**−16.5**

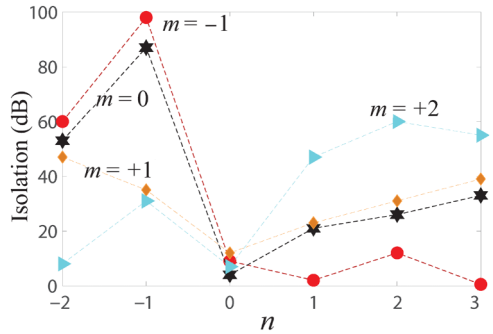

FIG. 13. Isolation between forward- and backward-diffracted orders achieved from the results in Figs. 12(a)–12(d).

$\theta_i = 35^\circ$ for forward incidence and $\theta_i = -35^\circ$ for backward incidence.

IV. APPLICATION OF STP GRATINGS TO MODERN WIRELESS COMMUNICATION SYSTEMS

The proposed STP grating offers unique properties that can be utilized for the realization of new types of electromagnetic devices and operations, such as, for instance, nonreciprocal beam shaping and beam coding, multifunctionality antennas, tunable and nonreciprocal beam steering, enhanced resolution holography, multiple images holography, illusion cloaking, etc.

Figure 14 presents an original application of the STP diffraction grating to wireless communications. Such a communication system is hereby called a space-time diffraction code multiple-access system. In the example provided in Fig. 14, we consider three pairs of transceivers (in practice, one may consider more pairs of transceivers). In such a scenario, only the transceiver pairs that share the same space-time diffraction pattern can communicate. Each diffraction pattern is attributed to the properties of the grating space-time modulation, i.e., the input frequency, where the input data (message) play the role of the modulation signal. For a specified set of input data (modulation signal), a unique diffraction pattern is created. In the particular example in Fig. 14, the transceiver pairs that are allowed to communicate are 1 and 1′, 2 and 2′, and 3 and 3′, so that the transceivers 2′ and 3′ (2 and 3) are incapable of retrieving the data sent by the transceiver 1 (1′), the transceivers 1′ and 3′ (1 and 3) are incapable of retrieving the data sent by the transceiver 2 (2′), and so forth. Each communication pair shares a certain space-time diffraction

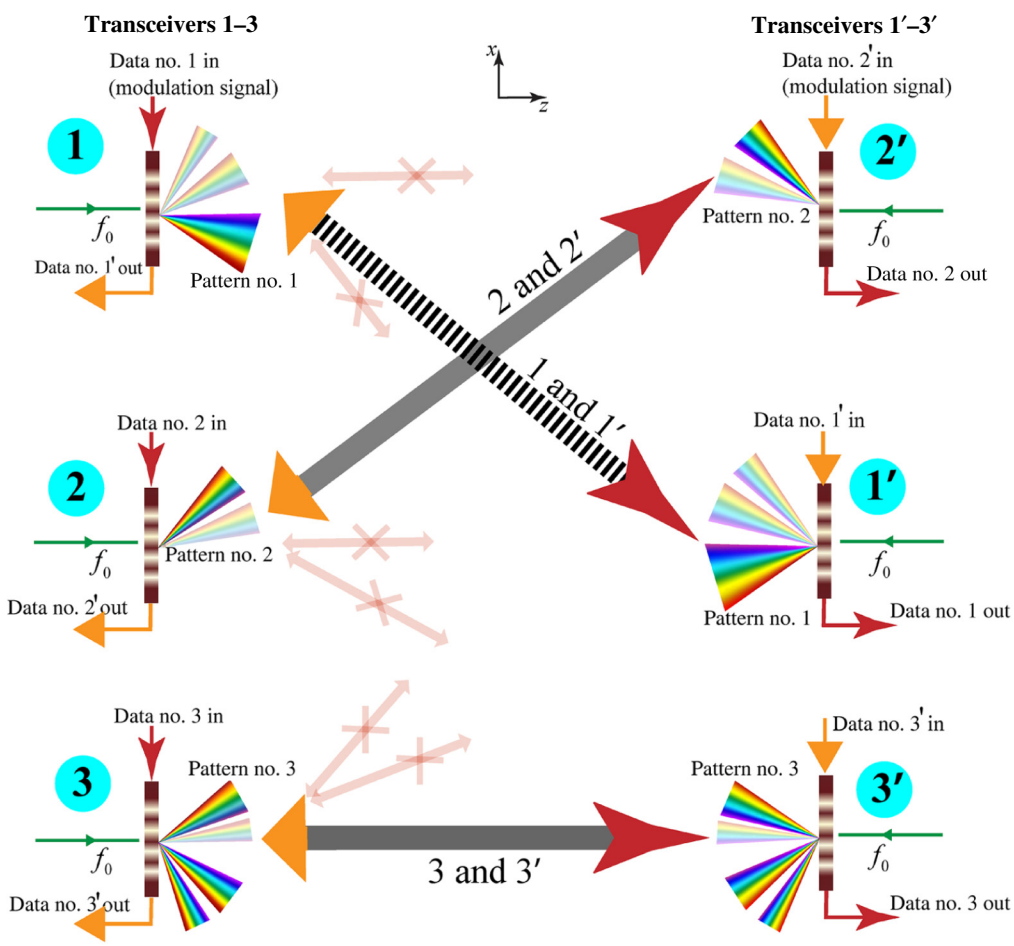

FIG. 14. Application of STP diffraction gratings to a full-duplex STDCMA system.

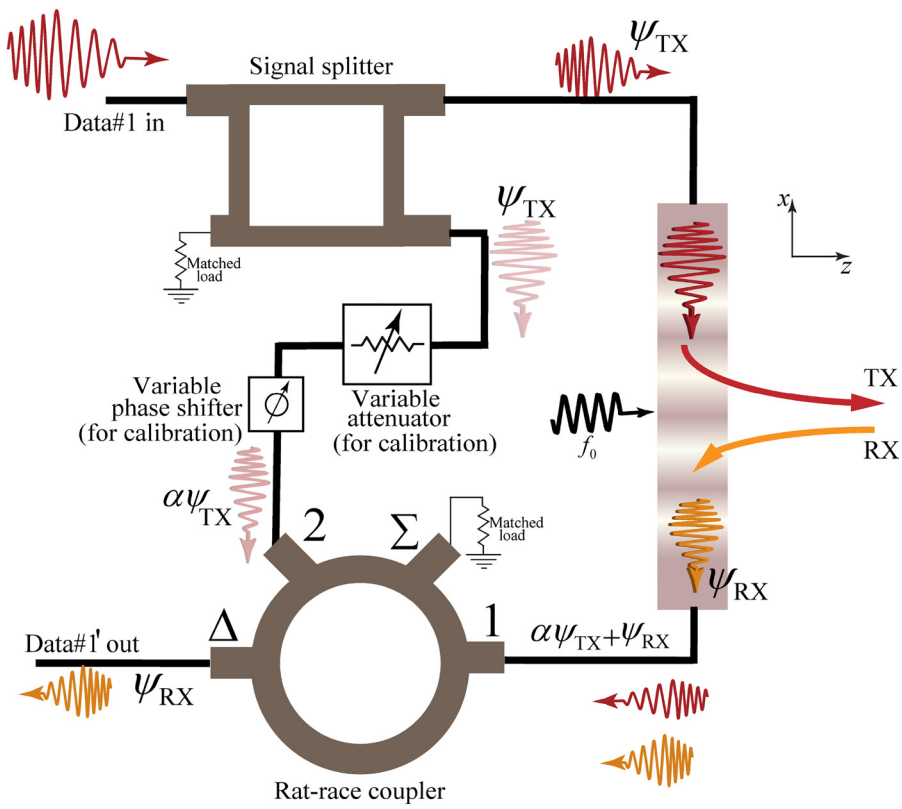

FIG. 15. Full-duplex operation of STP-diffraction-based transceivers in Fig. 14 based on unidirectional ($-x$ direction) traveling of both TX and RX signals, where complete cancellation of the TX signal in the RX port is enforced.

pattern. Each diffraction pattern can be created by certain space-time modulation parameters, e.g., δ_ϵ, ϵ_{av}, the K/Ω ratio, and the grating thickness d. Since the radiation pattern provided by a STP diffraction grating is very diverse and is very sensitive to the space-time modulation parameters, an optimal isolation between the transceivers can be achieved by proper design of the diffraction patterns.

Such a multiple-access scheme is endowed with full-duplex operation thanks to the unique nonreciprocity provided by the properties of a STP diffraction grating. Figure 15 depicts the architecture of a STP-diffraction-grating-based transceiver in the STDCMA system in Fig. 14. Such an architecture is composed of a STP diffraction grating illuminated by an incident wave with frequency f_0. In the transmit mode (TX), the grating is modulated by the input data denoted by ψ_{TX}, which is injected into the grating from the top and travels in the $-x$ direction. In the receive mode (RX), the incoming wave (which includes a set of spatial-temporal diffraction orders) impinges on the grating and, while interacting with the incident wave with frequency f_0, yields a $-x$ traveling wave inside the grating, denoted by ψ_{RX}. We stress that the ψ_{RX} signal traveling in the $-x$ direction is enforced by proper design of the grating, which is explained later.

As we see in Fig. 15, the signal wave at the receiver port is composed of the received signal (ψ_{RX}) plus a portion of the input data of the transmission mode ($\alpha\psi_{TX}$). To ensure complete cancellation of the ψ_{TX} in the receiver port, we may use the circuit in the left side of Fig. 15. This circuit is composed of a signal splitter that provides a sample from the input data of the transmit mode (ψ_{TX}), a variable attenuator, and a variable phase shifter for calibration purposes to provide $\alpha\psi_{TX}$. Then, the signal wave at the receiver port, i.e., $\psi_{RX} + \alpha\psi_{TX}$, is subtracted from the calibrated sample signal, that is, $\alpha\psi_{TX}$, by a rat-race coupler. Thus, the signal at the difference port of the rat-race coupler is the desired received signal ψ_{RX}. It is worth mentioning that the calibration of the architecture can be performed by disconnecting the RX port from port 1 of the rat-race coupler, connecting port 1 to a match load, and then seeking for a null at the difference port of the rat-race coupler by adjusting the variable attenuator and variable phase shifter, so that ψ_{TX} is completely canceled out at the difference port of the rat-race coupler.

An elegant feature of the transceiver scheme in Fig. 15 is that the diffraction grating is used as the receiver (as well as the transmitter), where the received signal wave acts as the modulation signal (specifies the K and Ω parameters) instead of the incident field. The key reason for the duplexing operation is that, inside the grating, the wave can only flow downstream. Figure 16 shows how the full-duplex operation is achieved by proper design of the diffraction grating, where only negative diffraction orders, i.e., $-x$ propagating orders, are generated, while positive diffraction orders, that is, $+x$ propagating orders, are evanescent. This way, we ensure that inside the grating,

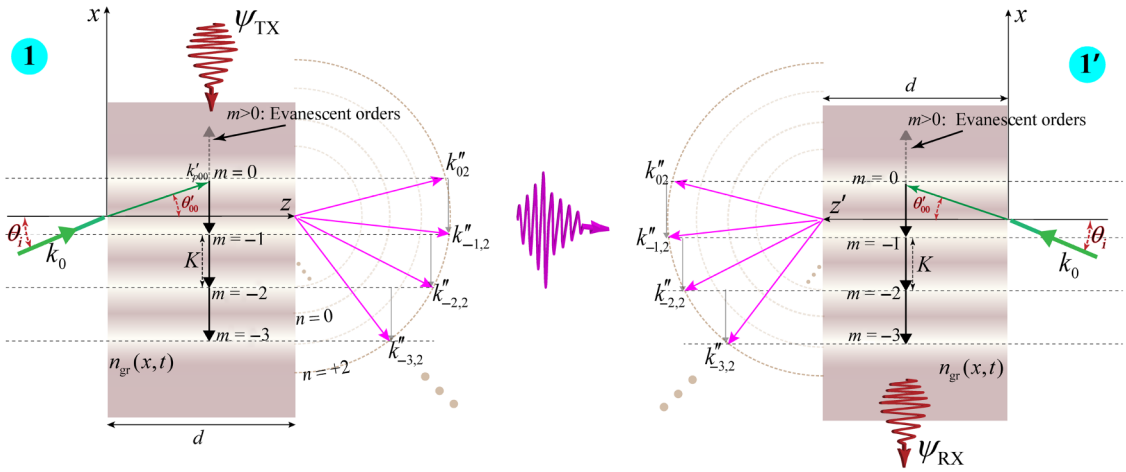

FIG. 16. Wave-vector diagram of a particular transceiver pair in the space-time diffraction code multiple-access system in Fig. 14.

all the diffraction orders are traveling in the $-x$ direction, in both the transmit and receive modes. In Fig. 16, transceiver 1 operates in the transmit mode, where the input data (ψ_{TX}) are injected into the grating from the top and, while interacting with the incident wave with the wave number k_0, generate a number of nonpositive diffraction orders, i.e., $m \geq 0$. In the right side of Fig. 16, transceiver 1′ receives the diffracted orders by transceiver 1, so that the resultant wave inside ψ_{RX} exits the grating from the bottom port of the grating, as all the diffraction orders can only travel in the $-x$ direction.

V. CONCLUSION

We present the analysis and characterization of space-time-periodic diffraction gratings as the generalized version of conventional spatially periodic diffraction gratings. Such STP gratings offer enhanced functionalities and exotic behavior. It is shown that such gratings provide an asymmetric diffraction pattern, nonreciprocal diffraction, and an enhanced diffraction efficiency, as well as frequency generation. Moreover, each spatial diffraction order includes an infinite set of temporal diffraction orders. We provide the theoretical investigation of the problem, which is supported by FDTD numerical simulation results. Such structures with marked differences with conventional spatially periodic diffraction gratings are expected to find interesting applications in optical and communication systems. As a particular example, we propose the space-time diffraction code multiple-access system as a promising communication system featuring full-duplex operation.

[1] T. K. Gaylord and M. G. Moharam, Planar dielectric grating diffraction theories, Appl. Phys. B **28**, 1 (1982).

[2] Theodor Tamir, H. C. Wang, and Arthur A. Oliner, Wave propagation in sinusoidally stratified dielectric media, IEEE Trans. Microw. Theory Tech. **12**, 323 (1964).

[3] C. B. Burckhardt, Diffraction of a plane wave at a sinusoidally stratified dielectric grating, J. Opt. Soc. Am. **56**, 1502 (1966).

[4] M. G. Moharam, Eric B. Grann, Drew A. Pommet, and T. K. Gaylord, Formulation for stable and efficient implementation of the rigorous coupled-wave analysis of binary gratings, J. Opt. Soc. Am. A **12**, 1068 (1995).

[5] Michael C. Hutley, *Diffraction Gratings (Techniques of Physics)* (Academic Press, London, 1982).

[6] Erwin G. Loewen and Evgeny Popov, *Diffraction Gratings and Applications* (CRC Press, Boca Raton, 1997).

[7] Craig Newswanger, Holographic diffraction grating patterns and methods for creating the same, U. S. Patent No. 5,291,317 (1994).

[8] Howard Michael Smith, *Holographic Recording Materials* (Springer Science & Business Media, New York, 2006), Vol. 20.

[9] W. B. Veldkamp, Laser beam profile shaping with interlaced binary diffraction gratings, Appl. Opt. **21**, 3209 (1982).

[10] Kendall Preston, *Coherent Optical Computers* (McGraw-Hill, New York, 1972).

[11] P. Chavel, A. A. Sawchuk, T. C. Strand, A. R. Tanguay, and B. H. Soffer, Optical logic with variable-grating-mode liquid-crystal devices, Opt. Lett. **5**, 398 (1980).

[12] H. Eichler, G. Salje, and H. Stahl, Thermal diffusion measurements using spatially periodic temperature distributions induced by laser light, J. Appl. Phys. **44**, 5383 (1973).

[13] Donald W. Phillion, Dirk J. Kuizenga, and A. E. Siegman, Subnanosecond relaxation time measurements using a transient induced grating method, Appl. Phys. Lett. **27**, 85 (1975).

[14] D. L. Hecht, Spectrum analysis using acousto-optic devices, Opt. Eng. **16**, 165461 (1977).

[15] T. Suhara, H. Nishihara, and J. Koyama, A folded-type integrated-optic spectrum analyzer using butt-coupled chirped grating lenses, IEEE J. Quantum Electron. **18**, 1057 (1982).

[16] Thomas K. Gaylord and M. G. Moharam, Analysis and applications of optical diffraction by gratings, Proc. IEEE **73**, 894 (1985).

[17] Edward S. Cassedy, in *Proceedings of the Institution of Electrical Engineers* (IET, 1965), Vol. 112, p. 269.

[18] E. S. Cassedy, Dispersion relations in time-space periodic media: Part II-unstable interactions, Proc. IEEE **55**, 1154 (1967).

[19] Sajjad Taravati, Nima Chamanara, and Christophe Caloz, Nonreciprocal electromagnetic scattering from a periodically space-time modulated slab and application to a quasisonic isolator, Phys. Rev. B **96**, 165144 (2017).

[20] Sajjad Taravati, Giant Linear Nonreciprocity, Zero Reflection, and Zero Band Gap in Equilibrated Space-time-varying Media, Phys. Rev. Appl. **9**, 064012 (2018).

[21] Sajjad Taravati and Ahmed A. Kishk, Advanced wave engineering via obliquely illuminated space-time-modulated slab, IEEE Trans. Antennas Propagat. **67**, 270 (2019).

[22] Sandeep Inampudi, Mohammad Mahdi Salary, Samad Jafar-Zanjani, and Hossein Mosallaei, Rigorous space-time coupled-wave analysis for patterned surfaces with temporal permittivity modulation, Opt. Mater. Express **9**, 162 (2019).

[23] Sameh Y. Elnaggar and Gregory N. Milford, Generalized space-time periodic circuits for arbitrary structures, arXiv:1901.08698 (2019).

[24] Sajjad Taravati and Ahmed A. Kishk, Dynamic modulation yields one-way beam splitting, Phys. Rev. B **99**, 075101 (2019).

[25] Neng Wang, Zhao-Qing Zhang, and C. T. Chan, Photonic floquet media with a complex time-periodic permittivity, Phys. Rev. B **98**, 085142 (2018).

[26] Sajjad Taravati and Ahmed A. Kishk, Space-time modulation: Principles and applications, arXiv:1903.01272 (2019).

[27] Jorge R. Zurita-Sánchez, P. Halevi, and Juan C. Cervantes-Gonzalez, Reflection and transmission of a wave incident on a slab with a time-periodic dielectric function, Phys. Rev. A **79**, 053821 (2009).

[28] Juan Sabino Martínez-Romero and P. Halevi, Parametric resonances in a temporal photonic crystal slab, Phys. Rev. A **98**, 053852 (2018).

[29] Mohammad Mahdi Salary, Samad Jafar-Zanjani, and Hossein Mosallaei, Time-varying metamaterials based on graphene-wrapped microwires: Modeling and potential applications, Phys. Rev. B **97**, 115421 (2018).

[30] Zhanni Wu and Anthony Grbic, in *2018 12th International Congress on Artificial Materials for Novel Wave Phenomena (Metamaterials)* (IEEE, Espoo, 2018), p. 439.

[31] P. K. Tien, Parametric amplification and frequency mixing in propagating circuits, J. Appl. Phys. **29**, 1347 (1958).

[32] E. S. Cassedy and A. A. Oliner, Dispersion relations in time-space periodic media: Part I-stable interactions, Proc. IEEE **51**, 1342 (1963).

[33] Z. Yu and S. Fan, Complete optical isolation created by indirect interband photonic transitions, Nat. Photonics **3**, 91 (2009).

[34] Junfei Li, Chen Shen, Xiaohui Zhu, Yangbo Xie, and Steven A. Cummer, Nonreciprocal sound propagation in space-time modulated media, Phys. Rev. B **99**, 144311 (2019).

[35] Mourad Oudich, Yuanchen Deng, Molei Tao, and Yun Jing, Space-time phononic crystals with anomalous topological edge states, arXiv:1904.02711 (2019).

[36] A. L. Cullen, A travelling-wave parametric amplifier, Nature **181**, 332 (1958).

[37] P. K. Tien and H. Suhl, A traveling-wave ferromagnetic amplifier, *Proc. IEEE* 46, 700 (1958).

[38] J. L. Wentz, A nonreciprocal electrooptic device, Proc. IEEE **54**, 97 (1966).

[39] Suhas Bhandare, Selwan K. Ibrahim, David Sandel, Hongbin Zhang, F. Wust, and Reinhold Noé, Novel nonmagnetic 30-dB traveling-wave single-sideband optical isolator integrated in III/V material, IEEE J. Sel. Top. Quantum Electron. **11**, 417 (2005).

[40] H. Lira, Z. Yu, S. Fan, and M. Lipson, Electrically Driven Nonreciprocity Induced by Interband Photonic Transition on a Silicon Chip, Phys. Rev. Lett. **109**, 033901 (2012).

[41] Nicholas A. Estep, Dimitrios L. Sounas, Jason Soric, and Andrea Alù, Magnetic-free non-reciprocity and isolation based on parametrically modulated coupled-resonator loops, Nat. Phys. **10**, 923 (2014).

[42] Sajjad Taravati, Self-biased broadband magnet-free linear isolator based on one-way space-time coherency, Phys. Rev. B **96**, 235150 (2017).

[43] Y. Hadad, D. L. Sounas, and A. Alù, Space-time gradient metasurfaces, Phys. Rev. B **92**, 100304 (2015).

[44] Y. Shi and S. Fan, Dynamic non-reciprocal meta-surfaces with arbitrary phase reconfigurability based on photonic transition in meta-atoms, Appl. Phys. Lett. **108**, 021110 (2016).

[45] Yu Shi, Seunghoon Han, and Shanhui Fan, Optical circulation and isolation based on indirect photonic transitions of guided resonance modes, ACS Photonics **4**, 1639 (2017).

[46] Mohammad Mahdi Salary, Samad Jafar-Zanjani, and Hossein Mosallaei, Electrically tunable harmonics in time-modulated metasurfaces for wavefront engineering, New J. Phys. **20**, 123023 (2018).

[47] Lei Zhang, Xiao Qing Chen, Shuo Liu, Qian Zhang, Jie Zhao, JunYan Dai, Guo Dong Bai, Xiang Wan, Qiang Cheng, Giuseppe Castaldi, Vincenzo Galdi, and Tie Jun Cui, Space-time-coding digital metasurfaces, Nat. Commun. **9**, 4334 (2018).

[48] Sajjad Taravati, Aperiodic space-time modulation for pure frequency mixing, Phys. Rev. B **97**, 115131 (2018).

[49] H. Shanks, A new technique for electronic scanning, IEEE Trans. Antennas Propag. **9**, 162 (1961).

[50] S. Taravati and C. Caloz, in *IEEE AP-S Int. Antennas Propagat. (APS)* (IEEE, Vancouver, Canada, 2015).

[51] Y. Hadad, J. C. Soric, and A. Alù, Breaking temporal symmetries for emission and absorption, Proc. Natl. Acad. Sci. **113**, 3471 (2016).

[52] Davide Ramaccia, Dimitrios L. Sounas, Andrea Alù, Filiberto Bilotti, and Alessandro Toscano, Nonreciprocity in antenna radiation induced by space-time varying metamaterial cloaks, IEEE Antennas Wirel. Propagat. Lett. **17**, 1968 (2018).

[53] Sajjad Taravati and Ahmed A. Kishk, in *2018 18th International Symposium on Antenna Technology and Applied Electromagnetics (ANTEM)* (IEEE, Waterloo, 2018), p. 1.

[54] Mohammad Mahdi Salary, Jafar-Zanjani Samad, and Hossein Mosallaei, Nonreciprocal optical links based on

time-modulated nanoantenna arrays: Full-duplex communication, Phys. Rev. B **99**, 045416 (2019).

[55] Amir Shlivinski and Yakir Hadad, Beyond the Bode-fano Bound: Wideband Impedance Matching for Short Pulses Using Temporal Switching of Transmission-line Parameters, Phys. Rev. Lett. **121**, 204301 (2018).

[56] Sajjad Taravati and Christophe Caloz, Mixer-duplexer-antenna leaky-wave system based on periodic space-time modulation, IEEE Trans. Antennas Propagat. **65**, 442 (2017).

[57] D. Correas-Serrano, A. Alù, and J. S. Gomez-Diaz, Magnetic-free nonreciprocal photonic platform based on time-modulated graphene capacitors, Phys. Rev. B **98**, 165428 (2018).

[58] Mingkai Liu, David A. Powell, Yair Zarate, and Ilya V. Shadrivov, Huygens' Metadevices for Parametric Waves, Phys. Rev. X **8**, 031077 (2018).

[59] S. Taravati and Ahmed A. Kishk, in *2018 12th International Congress on Artificial Materials for Novel Wave Phenomena (Metamaterials)* (IEEE, Espoo, 2018), p. 383.

[60] M. G. Moharam and T. K. Gaylord, Three-dimensional vector coupled-wave analysis of planar-grating diffraction, J. Opt. Soc. Am. **73**, 1105 (1983).

[61] Yadong Xu, Yangyang Fu, and Huanyang Chen, Steering light by a sub-wavelength metallic grating from transformation optics, Sci. Rep. **5**, 12219 (2015).

[62] Nicolas Bonod and Jérôme Neauport, Diffraction gratings: from principles to applications in high-intensity lasers, Adv. Opt. Photonics **8**, 156 (2016).

[63] Mohammad Memarian and George V. Eleftheriades, Evanescent-to-propagating wave conversion in sub-wavelength metal-strip gratings, IEEE Trans. Microw. Theory Techn. **60**, 3893 (2012).

[64] Mohammad Memarian and George V. Eleftheriades, Enhanced radiation of an invisible array of sources through a sub-wavelength metal-strip grating and applications, J. Appl. Phys. **114**, 134902 (2013).

[65] Vladislav Popov, Fabrice Boust, and Shah Nawaz Burokur, Controlling Diffraction Patterns with Metagratings, Phys. Rev. Appl. **10**, 011002 (2018).

[66] Vladislav Popov, Fabrice Boust, and Shah Nawaz Burokur, Constructing the near Field and far Field with Reactive Metagratings: Study on the Degrees of Freedom, Phys. Rev. Appl. **11**, 024074 (2019).

[67] L. Felsen and G. Whitman, Wave propagation in time-varying media, IEEE Trans. Antennas Propag. **18**, 242 (1970).

[68] Fabio Biancalana, Andreas Amann, Alexander V. Uskov, and Eoin P. O'reilly, Dynamics of light propagation in spatiotemporal dielectric structures, Phys. Rev. E **75**, 046607 (2007).

[69] Vincent Bacot, Matthieu Labousse, Antonin Eddi, Mathias Fink, and Emmanuel Fort, Time reversal and holography with spacetime transformations, Nat. Phys. **12**, 972 (2016).

[70] Frederic R. Morgenthaler, Velocity modulation of electromagnetic waves, IEEE Trans. Microw. Theory Tech. **6**, 167 (1958).

[71] R. Fante, Transmission of electromagnetic waves into time-varying media, IEEE Trans. Antennas Propagat. **19**, 417 (1971).

[72] Zoé-Lise Deck-Léger, Scattering in space-time abruptly modulated structures, Ph.D. thesis, École Polytechnique de Montréal (2017).

[73] R. C. Costen and D. Adamson, Three-dimensional derivation of the electrodynamic jump conditions and momentum-energy laws at a moving boundary, Proc. IEEE **53**, 1181 (1965).

[74] B. M. Bolotovskiĭ and S. N. Stolyarov, Reflection of light from a moving mirror and related problems, Sov. Phys. Usp. **32**, 813 (1989).

[75] E. S. Cassedy and A. A. Oliner, Dispersion relations in time-space periodic media: Part I: Stable interactions, Proc. IEEE **51**, 1342 (1963).

[76] Dimitrios L. Sounas and Andrea Alù, Non-reciprocal photonics based on time modulation, Nat. Photonics **11**, 774 (2017).

[77] Christophe Caloz, Andrea Alù, Sergei Tretyakov, Dimitrios Sounas, Karim Achouri, and Zoé-Lise Deck-Léger, Electromagnetic Nonreciprocity, Phys. Rev. Appl. **10**, 047001 (2018).

[78] Aurélien Merkel, Morten Willatzen, and Johan Christensen, Dynamic Nonreciprocity in Loss-compensated Piezophononic Media, Phys. Rev. Appl. **9**, 034033 (2018).

[79] V. A. Fedotov, P. L. Mladyonov, S. L. Prosvirnin, A. V. Rogacheva, Y. Chen, and N. I. Zheludev, Asymmetric Propagation of Electromagnetic Waves through a Planar Chiral Structure, Phys. Rev. Lett. **97**, 167401 (2006).

[80] R. Singh, E. Plum, C. Menzel, C. Rockstuhl, A. K. Azad, R. A. Cheville, F. Lederer, W. Zhang, and N. I. Zheludev, Terahertz metamaterial with asymmetric transmission, Phys. Rev. B **80**, 153104 (2009).

[81] Liang Feng, Maurice Ayache, Jingqing Huang, Ye-Long Xu, Ming-Hui Lu, Yan-Feng Chen, Yeshaiahu Fainman, and Axel Scherer, Nonreciprocal light propagation in a silicon photonic circuit, Science **333**, 729 (2011).

[82] Shanhui Fan, Roel Baets, Alexander Petrov, Zongfu Yu, John D. Joannopoulos, Wolfgang Freude, Andrea Melloni, Miloš Popović, Mathias Vanwolleghem, Dirk Jalas, Manfred Eich, Michael Krause, Hagen Renner, Ernst Brinkmeyer, and Christopher R. Doerr, Comment on "nonreciprocal light propagation in a silicon photonic circuit", Science **335**, 38 (2012).

[83] Xuchen Wang, Ana Díaz-Rubio, Viktar S. Asadchy, Grigorii Ptitcyn, Andrey A. Generalov, Juha Ala-Laurinaho, and Sergei A. Tretyakov, Extreme Asymmetry in Metasurfaces via Evanescent Fields Engineering: Angular-asymmetric Absorption, Phys. Rev. Lett. **121**, 256802 (2018).

[84] N. E. Glass, Nonreciprocal diffraction via grating coupling to surface magnetoplasmons, Phys. Rev. B **41**, 7615 (1990).

[85] O. G. Udalov, M. V. Sapozhnikov, E. A. Karashtin, B. A. Gribkov, S. A. Gusev, E. V. Skorohodov, V. V. Rogov, A. Yu Klimov, and A. A. Fraerman, Nonreciprocal light diffraction by a lattice of magnetic vortices, Phys. Rev. B **86**, 094416 (2012).

[86] Tian-Jing Guo, Teng-Fei Li, Mu Yang, Hai-Xu Cui, Qing-Hua Guo, Xue-Wei Cao, and Jing Chen, Nonreciprocal optical diffraction by a single layer of gyromagnetic cylinders, Opt. Express **22**, 537 (2014).

Correction: The previously published Figure 2(a) contained an error in one of the labels and has been replaced.